Investigation into the formation of the scrape-off layer density shoulder in JET ITER-like wall L-mode and H-mode plasmas

Investigation of the Scrape-off layer density shoulder formation in JET-ILW L-mode and H-mode Plasmas

A. Wynn[a], B. Lipschultz[a**], I. Cziegler[a], J. Harrison[b], A. Jaervinen[c] G. F. Matthews[b], J. Schmitz[a,d], B.Tal[e], M. Brix[b], C. Guillemaut[b,f], D. Frigione[g], A. Huber[d], E. Joffrin[h], U. Kruzei[b], F. Militello[b], A. Nielsen[i], S. N. Walkden[b], S. Wiesen[d] and JET contributors*

EUROfusion Consortium, JET, Culham Science Centre, Abingdon, OX14 3DB, UK

[a]York Plasma Institute, University of York, Heslington, York, YO10 5DD, UK
[b]CCFE ,Culham Science Centre, Abingdon, OX14 3DB, UK
[c]Lawrence Livermore National Laboratory, Livermore, California, USA
[d]Forschungszentrum Jülich Gmbh, Institut für Energie- und Klimaforschung - Plasmaphysik, 52425 Jülich, Germany
[e]Wigner Research Centre for Physics, HAS, P.O.B. 49, H - 1525 Budapest, Hungary
[f]Instituto de Plasmas e Fusao Nuclear, Universidade Lisboa, Portugal
[g]Associazione EURATOM-ENEA sulla Fusione, CP 65, Frascati, Rome, Italy
[h]Association EURATOM-CEA, CEA/DSM/DRFC CEA-Cadarache, 13108 Saint Paul Lez Durance, France
[i]Association Euratom DTU, Technical University of Denmark, PO Box 49, DK 4000 Roskilde, Denmark
*See the author list of "X. Litaudon et al 2017 Nucl. Fusion 57 102001
**Corresponding author e-mail: bruce.lipschultz@york.ac.uk

Abstract: The low temperature boundary layer plasma (Scrape-Off-Layer or SOL) between the hot core and the surrounding vessel determines the level of power loading and erosion and implantation of material surfaces, and thus the viability of tokamak-based fusion as an energy source. This study explores mechanisms affecting the formation of flattened density profiles, the so-called 'density shoulders', in the low-field side (LFS) SOL, which modify ion and neutral fluxes to surfaces – and the subsequent erosion. To do so we have covered a factor of two range in plasma current, compared the effect of vertical (closed) vs horizontal (open) outer divertor target configurations, as well as the effect of divertor nitrogen (N_2) seeding vs deuterium (D_2) fuelling for L-mode plasmas. There is evidence against local enhancement of ionization inducing shoulder formation. It is only in cases with D_2 fuelling, utilizing the horizontal target (tile 5) at the outer divertor, that increases in divertor parallel resistivity, as quantified by increases in far SOL Λ_{div} ($=[L_{||}n_{ei}\Omega_i]/c_s\Omega_e$), correlate with increases in SOL density shoulder amplitude, A_s. However, that correlation does not extend to increases in $\Lambda_{div,}$ induced by divertor N_2 seeding, indicating that increasing divertor resistivity is not a sufficient condition for shoulder growth. In contrast to parallel resistivity, the magnitude of Balmer D_α line emissivity near the strike point does scale with shoulder amplitude across both D_2 fuelling and N_2 seeding discharges. The divertor D_α emissivity can be related to both ionization and charge exchange

(CX) processes, both of which have been shown to modify parallel divertor flows and thus the loss of ions out of the SOL; a control on density upstream in the main chamber SOL. A comparitive study of H-mode discharges for plasmas leads to similar conclusions.

1. Introduction

Understanding the physics governing the intensity and nature of plasma interactions with vessel surfaces is critical to the attainment of fusion power in magnetically controlled devices. By design, next step fusion devices such as ITER, and likely future devices such as DEMO, will prevent the hot, fusing, confined plasma from directly contacting the vessel surfaces by using a divertor magnetic geometry ([1] and references therein). In an ideal divertor scenario, all of the energy and particles exiting the edge of the confined region, through what is known as the last closed flux surface (LCFS) or separatrix, are transported to the divertor region. This ideal generally holds for energy transport due to the dominance of energy transport parallel to magnetic field lines compared to the perpendicular direction, leading to high divertor power flux densities for attached H-mode plasmas [2]. Techniques have been developed to mitigate those high power fluxes by inducing divertor detachment [3, 4].

A number of studies have shown that there are still significant charge exchange neutral and anomalous cross-field ion fluxes to main chamber surfaces outside the divertor region [5-9]. Indeed, under detached divertor conditions, the divertor ion (and power) fluxes have been strongly reduced leaving the total ion flux to main chamber surfaces comparable to that to the divertor in both L-mode and H-mode plasmas [10]. Due to the large area of the main chamber walls the steady state ion and neutral heat flux densities there are small compared to the divertor.

This study addresses some characteristics of the SOL density profile with the ultimate goal of predicting, and hopefully reducing, the erosion and fuel retention of the first wall in a fusion reactor. The main causes of erosion to plasma facing components (PFCs, typically limiters) sputtering by a) radial ion fluxes; and b) the flux of high energy CX neutrals that are born inside the separatrix [9, 11-13]. For each sputtering erosion source the shape of the density profile and the mechanisms that control it are central. For example, when the scale length of the density gradient near main chamber surfaces (‘far SOL’) becomes large, often described as ‘shoulder’ formation’ [7, 14], the ion density at the limiter increases and the ion fluxes ($\propto nC_s$) to such surfaces rise strongly.

Shoulder formation and the resultant flattening of the far SOL density profile have been found to occur in several tokamaks in a variety of operating regimes [7, 8, 10, 14-19]. The initial observations by McCormick showed that the flattening in the far SOL occurred at high density and low current [14]. LaBombard [7] first coined the description of the 'near' and 'far' SOL along with defining a 'shoulder' as the break point in the density profile between the 'near' (near the separatrix) and 'far' (far from the separatrix) SOL (Herein we use the term 'shoulder' interchangeably with 'density shoulder' in the low-field side SOL). As the operating densities of such plasmas approached the global density limit [20], the flattened region moved towards the separatrix (sometimes called 'broadening'). The goal of the study presented in this paper is to examine various mechanisms that could lead to shoulder formation in the JET tokamak with the ITER-like Wall (ILW) where the main chamber limiter surfaces are Be and the divertor surfaces are tungsten[21].

Previous research into SOL cross-field transport showed that the flattened SOL density profiles are not consistent with diffusive transport, and that advection is the likely transport mechanism [7, 22-24]. Boedo [24] showed that turbulence accounted for up to 50% of the radial transport onto main chamber surfaces. LaBombard [24] found that flattening SOL density profiles correlated with larger amplitude fluctuations in the SOL as the core plasma density was increased on C-Mod. This relationship has been confirmed on a number of tokamaks including TCV [25], DIII-D [8], and MAST [26].
Despite the well-documented correlation, only recently have code and analytic models been advanced that appear to predict the statistical properties of SOL advection and the resultant time averaged density profiles [27-30].

Both experimental measurements and models show that advective transport is manifested as filamentary structures in the SOL [31] elongated along magnetic field lines, with lengths on the order of πqR(~10m), and narrow perpendicular to it, of order 5-10ρ_i (1-2cm) (larger in spherical tokamaks) [32]. Here, q is the safety factor, R is the major radius and ρ_i is the ion gyro-radius. Filaments travel both radially and poloidally at velocities in the range 500-1000m/s.

A common conjecture is that the effective electrical resistances both parallel and perpendicular to the magnetic field line within a filament influence its characteristics [33]. More specifically, the electrical disconnection from the divertor target sheath, occurring at high collisionality (so-called 'inertial regime'), has been tied to changes in filament characteristics (increased size and velocity), and thus increased advective transport [25, 34-36]. An expression of the divertor collisionality/resistance is given by [34]

$$\Lambda_{div} = \frac{L_{\parallel} \nu_{ei} \Omega_i}{c_s \Omega_e} = 3.4x10^{-19} \frac{L_{\parallel} n_e \Omega_i}{T_e^2} \quad (1)$$

where ν_{ei} is the electron-ion collision frequency, $L_{//}$ (m) is the magnetic connection length from the LFS (low-field side) mid-plane of the plasma to the divertor target, Ω_i(s^{-1}) and Ω_e(s^{-1}) are the gyro-frequency of ions and electrons respectively, c_s (m/s) is the sound speed, n_e (m^{-3}) is the electron density and T_e (eV) is the electron temperature.

The experimental correlation between increased SOL density profile flattening, increases in filament size and velocity and Λ_{div}, was demonstrated by Carralero [36] for ASDEX-Upgrade (outer divertor strike point on the vertical target) and JET (outer divertor strike point on the horizontal target (tile 5)) L-mode plasmas. Carralero found that increasing Λ_{div} past 1, using either D_2 fuelling or N_2 seeding led to further flattening of the SOL profile as evidenced by an increase in the effective density e-folding length, λ_n, in the upstream SOL. Expansion of the far SOL flattened region toward the separatrix was found for ASDEX-Upgrade as Λ_{div} was increased further. The concurrent increase in both the filament size and velocity, shown only for the case of D_2 fuelling, was proposed as the causal mechanism for SOL flattening and increase in radial flux.

The strong correlation between filament characteristics changes and shoulder formation in ASDEX-Upgrade L-mode vertical target plasmas is not universally found. Vianello [37], in studying turbulent transport in TCV L-mode, D_2 fuelled plasmas with an open, or horizontal target divertor, found that λ_n does *not* correlate strongly with Λ_{div} , nor is there a sudden increase in λ_n when Λ_{div} increases past 1 in all cases. Furthermore, flattened LFS SOL profiles (shoulders) were also observed at low Λ_{div}. The TCV work is also notable in that Λ_{div} was varied through both density and connection length scans.

The motion of filaments has been extensively characterized numerically. Significant progress has been made in modelling filaments, initiating from 2D slab geometries, extending to 3D slabs [30, 38, 39] and also tokamak relevant geometries [40, 41]. Direct comparisons between simulations and experiments have also been performed [42, 43]. Recently, neutrals have been included self-consistently in tokamak relevant turbulence simulations in limited configuration [44]; implementation of x-point geometry is in progress.

The LFS SOL density shoulder formation mechanisms addressed in this paper are as follows:

(a) The conditions at, or inside, the separatrix (n_e, T_e and gradients) are expected to define turbulent filament birth characteristics (filament size, frequency, velocity…) and thus could ultimately affect/modify shoulders in the far SOL.

(b) As a filament travels through the SOL there could be changes in the local filament characteristics driven by resistivity along the field to the divertor (quantified by $\mathbf{\Lambda}_{div}$).

(c) Changes in local sources (e.g. ionization in the main chamber), which increase/decrease density or

(d) Changes to sinks (parallel loss of ions along B to the divertor) could raise or lower the local density in the filaments or background plasma.

Similar discussions of the above mechanisms have appeared elsewhere [19, 28, 30, 45, 46].

Based on the results presented in this paper we find that mechanisms (a) – (c) are, individually, not sufficient to cause the formation of the SOL density shoulder.

More specifically, for (a) and (c), comparisons of discharges with the outer strike point located on the horizontal vs vertical target indicated that under the same core/separatrix conditions and main chamber neutral pressures, there is *no* shoulder formation for the vertical (closed) target operation, while there *are* shoulders formed for horizontal (open) target operation.

Turning to the effect of parallel resistivity on the upstream SOL density profile (mechanism b) we find that increases in $\mathbf{\Lambda}_{div}$ *are not sufficient* to predict or form a shoulder; whereas increases in $\mathbf{\Lambda}_{div}$ through D_2 fuelling correlate with increases in shoulder amplitude, the same variation in $\mathbf{\Lambda}_{div}$ driven by N_2 seeding has essentially no effect on upstream shoulder amplitude.

In comparison to parallel resistivity ($\mathbf{\Lambda}_{div}$), increases in the divertor Balmer D_α line emissivity magnitude and profile *do* increase with upstream shoulder amplitude under D_2 fuelling and *do not* increase with N_2 seeding. We point to ion-neutral interactions of the fuel species (using D_α as a proxy) as a way for the divertor plasma to decrease the ion flows out of the upstream SOL and thus help form the shoulder. This may be understood as a clogging of the drainage of plasma by the neutrals, such as described for the upstream SOL in [29].

We also present a brief study of SOL density shoulder characteristics during inter-ELM H-mode periods utilizing the horizontal target; shoulder formation behavior for both D_2 fuelling and N_2 seeding is essentially the same as for L-mode plasmas.

This paper is structured as follows. In section 2 the experimental setup is presented. Section 3 introduces basic quantitative measures of the SOL density shoulder characteristics and the effect of plasma current on the density profile. In section 4 the validity of $\mathbf{\Lambda}_{div}$ as a general control

parameter for the SOL density profile is investigated. In section 5 the role of mid-plane neutrals as an ion source is presented. In section 6, we present evidence that plasma-neutral interaction of the fuel species in the divertor region, indicated by D_α emission, is a more general correlator for SOL density profile changes than Λ_{div}. In section 7, a brief study of H-modes is presented including the effect of D_2 fuelling and N_2 seeding. Sections 8 and 9 discuss and summarize the primary results of the study.

2. Experimental Setup

2.1 Diagnostics

Figure 1 shows a poloidal cross-section of JET-ILW with the different horizontal (open or HT, on tile 5) and vertical (closed or VT, on tile 7) outer target magnetic configurations and relevant diagnostics. For clarity, a close up of the divertor region is shown in figure 2.

Measurement of the SOL density profile is central to this study and the JET Li beam diagnostic [47] provides absolutely calibrated density profiles from approximately the pedestal top to the limiter radius. The Li beam enters the upper half of the plasma as shown in figure 1. When mapped to the midplane along flux surfaces to compare with other measurements, the midplane spatial resolution is ~2.5mm. Profiles are provided with a time resolution of 10 ms. In most cases the Li beam density profiles are averaged over 100ms.

A Penning–type gauge is substantially recessed from the vessel leading to poor time response (we estimate ~ 1 second), but provides the best currently available measurement of pressure at the midplane.

Divertor Langmuir probes (DLPs) provided target profiles of J_{sat}, n_e and T_e measurements across divertor surfaces at 100Hz, while J_{sat} was also available at 100 kHz. In L-mode cases, strike point sweeping of 4Hz and 1Hz frequency, in HT and VT respectively, with an amplitude of ~2.5cm, was used to provide fully resolved profiles of plasma characteristics across the divertor. However, not all probes on the HT were functional for the discharges in this study. That leads to data missing over sections of the divertor profile. Strike point sweeping was not used for H-mode cases.

Several gas injection locations were used for L-mode plasmas: GIM 11 (see figure 1) was always used for D_2 injection into the private flux region (PFR). However, GIM 9 moves from the common to private flux regions of the divertor plasma in shifting the equilibrium from HT to VT. GIM 9 was used for N_2 seeded discharges. GIM 10 injects into the common flux region in all cases.

In the case of H-mode plasmas GIMs 10 and 11 were used for D_2 injection while GIM 9 was used for N_2 seeding.

Optical cameras, filtered for emission lines including D_α, were also employed for both upstream SOL and divertor measurements of local D_α emissivity (through inversions of brightness images) in 1D (upstream SOL) and 2D in the divertor [48] respectively. For upstream SOL inversions, figure 1 shows the location of the radial D_α emissivity measurement points, which are a subset of data from the main chamber viewing 1000x1000 pixel CCD camera (80 degree field of view) system ('KL1 system'). Lines of sight tangential to flux surfaces at a fixed Z were selected by mapping pixel locations to vessel structures[49]. This brightness profile is then Abel inverted to provide a D_α emissivity profile which, when multiplied by the S/XB coefficient, gives the local ionization source, S_{ion}. The S/XB coefficient is taken from ADAS [50] and is dependent on the local T_e and n_e. The S/XB coefficient has not been modified to take into account molecules. SOL T_e measurements are not available in JET which led us to assume an exponential profile starting at 100eV at the separatrix, based on power balance and Thomson measurements. The assumed T_e decay length (2 cm) across the SOL and T_e at the limiter radius (10 eV) are based on past scanning Langmuir probe measurements from similar pulses. The sensitivity of the derived ionization rate to the above assumptions is small compared to D_α emissivity uncertainties; the S/XB coeffcients for interpreting the local D_α emissivity as an ionization rate are not sensitive to T_e above 10eV. Therefore, the profile shape should not influence the inferred S_{ion} strongly. An analysis of the sensitivity has been performed in [46]. 2D inversions of the divertor images were produced from dedicated cameras ('KL11') which view the divertor region tangentially, each camera filtered for a different spectral line including D_α and NII (line radiation from nitrogen ion at 451 nm) [13].

Another measure of the divertor D_α level and extent is through a set of vertically-viewing spectrometer chords shown in figure 2. Each of 5 chords spanning the HT target provides the brightness integrated through the SOL at the top of the machine and the divertor, which is the dominant component due to the low-triangularity configuration used (recycling from the top baffle is negligible). We utilize both the individual chords and the integral of their brightnesses across the divertor, I-D_α.

3. Basic Characterization of shoulder formation

3.1 The shoulder amplitude metric

We define here a simple new metric of the SOL density shoulder amplitude and location based upon normalizing each SOL density profile to its separatrix value. The method, whereby we

extract the shoulder peak amplitude and location from the Li beam data, is illustrated in figure 3. The horizontal co-ordinate, r-r_{sep}, is referenced to the mid-plane where r_{sep} is the separatrix radius. We utilize the SOL density profile at a time when the divertor is in sheath-limited (SL) regime (as discussed later, there is an absence of measurable SOL density shoulders in JET in the SL regime) as the reference profile shape (a). This reference profile and all subsequent profiles are also normalized to their separatrix values (b) and their difference to the reference profile is then the measured shoulder profile (c). The maximum of the normalized difference profile is our definition of the shoulder amplitude, A_s, while the location of the peak, r_{As}, is used to follow shoulder expansion towards the limiter (e.g. orange diamonds and black stars in figure 3 b and c). The above method is used for all plasmas studied in this work.

3.2 Dependence of the shoulder on density and plasma current

McCormick, in the first characterization of density shoulders [14], found that SOL density shoulder grew (became flatter) as the line average density, $\overline{n}_e$, was increased (for fixed plasma current, I_p), and the shoulder shoulder decreased as I_p was increased. We generally find the same trends for JET density scans (figure 3 (b)). We also find that increasing the plasma current by a factor of two at fixed $\overline{n}_e$ (figure 4 (a)) reduces, or suppresses the shoulder as McCormick observed. The near SOL density profile is characterized by an e-folding length of λ_n~ 2cm in all the cases of figures 3 and 4, typical for a wide range of plasmas studied in this paper. We note that as the SOL density profile returns to a single exponential profile, the ion current profile at the target (figure 4 (b)) changes as well – the peak current drops, indicating a less high-recycling divertor. The horizontal co-ordinate in figure 4 (b) has been mapped to the mid-plane for comparison with upstream profiles. Regions where r-r_{sep} <0 are in the PFR.

As can be observed from figure 3 (c) the location of the shoulder peak moves, or radial extent of the shoulder flattened (large λ_n) region extends outward with increasing core density after the shoulder is fully formed. Such changes strongly increase the density at the limiter radius and thus the ion fluxes to the limiters. Thus, there is first the formation of the shoulder (blue squares to green triangles), followed by an expansion phase (red stars to cyan circles).

4. The correlation of Λ_{div} with shoulder formation and growth

4.1 L-mode plasmas utilizing the outer divertor HT and D_2 fuelling

It is *only* with use of the outer divertor HT in Ohmically heated, D_2 fuelled, L-mode plasmas that enhanced parallel resistivity correlates generally with the flattening of the upstream density

profile; other pulse types detailed later in section 4 do not exhibit this correlation. While data was accumulated from 4 pulses at 4 different plasma currents we will only discuss the 2.5MA case (JPN89346) for clarity. Pulses for all currents from 1.5-3 MA reached detached divertor conditions – defined here as the outer divertor target density at the separatrix reached a maximum and then decreased. The core density is increased far past divertor detachment in all cases.

In general, we find that the *shoulder appears, or its amplitude is measureable, just after the divertor plasma transitions from sheath-limited (SL) to high-recycling (HR) conditions.* We define the beginning of the HR regime as the time when the values of density (temperature) and ion current near the separatrix start to increase (decrease) strongly as the core density is increased. One example of the transition to the HR regime is shown in figure 5 where colours and symbols correspond to specific times and $\bar{n}_e$ consistently across all sub-figures as well as the time traces in figure 6. Figure 5(a) displays SOL density profiles from the Li beam mapped to the mid-plane and normalized to the separatrix density (see section 3.1). Uncertainties are not shown but are similar to those shown in figure 4. At low densities (blue squares) SL conditions exist at the outer divertor HT with $T_{e,sp}$=35eV (d) and $n_{e,sep}$=6x10^{18}m^{-3} (b). The corresponding upstream density profile (a) is approximately exponential from separatrix to limiter. The next time point (magenta triangles) corresponds to higher core and divertor densities, the latter rising rapidly under HR conditions and the shoulder begins to form; the peak temperature and density at the target are T_e≈15eV and $n_{e,sep}$=2-3x10^{19} m^{-3}, respectively. As the core density is increased still further, the divertor plasma becomes increasingly high recycling (green circles, orange diamonds) and the shoulder magnitude continues to increase. At the highest densities (black pentagon symbols) the divertor starts to detach (density at strike point reduces slightly) and, while the shoulder amplitude is not increasing, the shoulder peak location moves radially towards the limiter ($r-r_{sep}$ = 5 cm), raising the density at the limiter radius.

Figure 5 (c) displays the profiles of Λ_{div} at the divertor target plate and how it changes dramatically through the transition from SL to HR regimes with further increases as the divertor becomes more high-recycling. The transition from SL to HR also corresponds to Λ_{div}, rising from below 1 to >10; this increase is more rapid than for the underlying target density and temperature due to the nonlinear dependence of Λ_{div} on those local plasma characteristics (eq. 1). The correlation between shoulder formation, the transition from SL to HR regimes and Λ_{div} was observed for all HT L-mode $\bar{n}_e$ scans at different values of I_p.

To emphasize the strong correlation of the transition from divertor SL to HR conditions with shoulder formation, figure 6 displays time traces of the quantities shown in figure 5. Values and error bars shown are moving averages and standard deviations over 100ms respectively – except

Λ_{div} where the error is propagated from the underlying n_e and T_e profiles as described. The uncertainties at individual time points are small compared to the error bars shown.

The transition of the divertor from sheath-limited to high-recycling occurs in figure 6 a at ~9.3s, just before the magenta line and triangle markers, as the lower uncertainty of A_s rises above 0. At that time Λ_{div} is in the range of 1-3. After the shoulder appears, A_s increases rapidly to 0.20 while Λ_{div} essentially saturates at values near 50. We note that the saturation of Λ_{div} is at least partially due to T_e saturating at values near 5eV, a common issue for Langmuir probe measurements in tokamaks [51]. $\Lambda_{div,far}$ follows a similar trend to $\Lambda_{div,near}$ but with slightly lower values and larger uncertainties. Gaps in the data are due to strike point sweeping.

The divertor and SOL data from all 4 plasma currents exhibit the same rapid increase in shoulder amplitude, A_s, as $\Lambda_{div,near}$ or $\Lambda_{div,far}$ increase above approximately 1 and divertor (and parallel transport) transitions from SL to HR. The relationship between A_s, and $\Lambda_{div,}$ is shown in figure 7 for the two cases of the abscissa being $\Lambda_{div,near}$ (a) and $\Lambda_{div,far}$ (b). The 4 pulses shown span the range of I_p=1.5-3.0 MA for the HT. *Most importantly, the relationship between A_s*, and $\Lambda_{div,}$ *appears to be independent of I_p. In addition, we find that a shoulder forms when Λ_{div} exceeds ~1-3 in either the near or far SOL regions.* The appearance of a shoulder above Λ_{div} ~1-3 is similar to the L-mode, vertical target, results from ASDEX-Upgrade [36] where the divertor detaches, as opposed to transitioning to HR. The relationship of the shoulder behavior reported in this paper to previous results will be expanded upon in the discussion section.

While Λ_{div} may generally correlate with A_s, the radial location of the shoulder peak, r_{As}, does not. Results are given in figure 8. During the period when the shoulder forms and grows in amplitude ($\Lambda_{div,near}$ <20-40), r_{As} stays essentially constant for the various plasma currents (figure 8 (a)), 1.8-2.4cm away from the separatrix. At $\Lambda_{div,near}$ >40, the divertor plasma is detached and a second phase is entered where r_{As} increases and A_s stays ~ constant, the second growth phase referred to earlier in the paper. The dependence of r_{As} on core plasma parameters, $\overline{n}_e$ and $\overline{n}_e/n_{gw}$ (figures 8 (b and c)), is more gradual, not indicating two phases as in figure 8 (a) because the divertor plasma is detached over most of the range in $\overline{n}_e$ plotted. The gradual increase in r_{As} with increasing $\overline{n}_e$ also suggests that the drop off in density outside of r_{As} (the second change of scale length) is not due to a limiter or other surface limiting the plasma.

4.2 L-mode plasmas utilizing the outer divertor VT and D_2 fuelling

One goal of this study was to determine whether the divertor configuration leads to any changes in divertor conditions and thus in SOL shoulder formation and growth. We know from both

modeling and experimental studies that divertor geometry (e.g. VT vs HT) can modify the detachment threshold in upstream density [52-54]. Furthermore, given variations in recycling properties between VT and HTs, there could be differences in the resistivity profile across the divertor target. JET presents an important opportunity to study the effect of the divertor configuration on shoulder formation and characteristics given its fairly unique capability to shift from one configuration to the other with minimal changes in the core plasma.

The L-mode discharges which utilize the VT in our study were operated with the same $\overline{n}_e$ scans for different plasma currents as for the HT data of the previous section. Time traces for the 1.5 MA VT pulse used in this section are shown in figure 9. As for the HT cases, there is a D_2 fuelling ramp (b) that results in a $\overline{n}_e$ ramp (a). The strike point density (c) rises quickly until ~ 10.5s, after which the density stops rising and then drops. We display the SOL density as well as divertor profiles in figure 10 for the same 1.5 MA case of figure 9. The symbols correspond to the same times in both figures. The outer gaps were 5cm, the same as for the HT cases. The values of $\overline{n}_e$ and the separatrix density were similar to those in figure 5 for the HT.

A small but discernable SOL density shoulder appears for operation with the VT. However, this occurs only at the highest $\overline{n}_e$ when the divertor is very detached. In difference to the HT case, $\Lambda_{div,near}$ and $\Lambda_{div,far}$ have significantly different values; $\Lambda_{div,near}$ *reaches values of order 100 as* the ion current to the target rolls over (not shown) and the peak divertor density decreases (black diamonds), which indicate detachment. In contrast $\Lambda_{div,far}$ is of order 1-10 when the shoulder forms and thus that region of the divertor is not detached. Another difference to operation with the HT is that the *divertor* density profile in the far SOL broadens substantially (figure 10(b)).

The different correlation of $\Lambda_{div,far}$ and $\Lambda_{div,far}$ with A_s is shown more clearly for the same pulse in figure 11. Unlike the case for operation with VT, A_s does not increase further when $\Lambda_{div,far}$ increases above 10. In summary, for VT operation, $\Lambda_{div,near}$ is a poor predictor of shoulder formation. And even though $\Lambda_{div,far}$ roughly shows the same Λ_{div} threshold for shoulder formation as for the HT, the shoulder growth is minimal and general behavior is very different than for the HT.

4.3 Nitrogen seeding to increase parallel resistivity

In the previous 2 sections, we reviewed the results obtained when D_2 fuelling was used to change the divertor conditions while simultaneously changing the upstream conditions ($\overline{n}_e$, $n_{e,sep}$, midplane pressure). To complement those studies, we have utilized a N_2 seeding ramp (figure 12 c) to directly modify the HT divertor conditions while holding upstream conditions such

as $\overline{n}_e$ (figure 12 a) roughly constant through constant D_2 fuelling (figure 12 b). The divertor is in a HR condition with a small shoulder even before the N_2 seeding commences. This is followed by detachment occurring after 13 seconds (~strike point density in figure 12 c dropping) as the N_2 seeding is increased.

Moving the divertor condition from HR to detachment by N_2 seeding leads to almost no change to the upstream SOL density profile. This is in stark contrast to the results of section 4.1 where there was a strong correlation between A_s and Λ_{div}, calculated for the near or far SOL. Figure 13 shows the usual upstream density and divertor profiles for an I_p = 2.5 MA plasma with N_2 seeding and a HT (discharge JPN90697). The symbols and colors correspond to those shown in figure 12. The SOL density profiles (figure 13 a) are not normalized to the separatrix density, unlike previous sections, since the core and separatrix densities hardly vary. The blue squares are the reference profile data from before N_2 injection, when the divertor plasma is in SL conditions as evidenced by low densities and high temperatures.

Prior to N_2 seeding the D_2 fuelling was increased by a factor of 3 to 4 and a small SOL density shoulder forms (green triangles) corresponding to the divertor near SOL being slightly high-recycling. Following the formation of this small shoulder, N_2 injection is initiated which leads the divertor to become even more high-recycling (red circles). Despite this large change in the divertor conditions as well as $\Lambda_{div,near}$ and $\Lambda_{div,far}$, there is very little variation in the SOL density profiles. Finally, at the highest levels of N_2 seeding (gold stars), detachment has begun.
Detachment with N_2 seeding (Λ_{div}~20-40) corresponds to *a reduction of the shoulder amplitude as well as a shift in the peak shoulder amplitude outward in major radius* by roughly 1 cm. This is in contrast to strictly D_2 fuelling (Section 3.1, figure 5) where the shoulder amplitude, A_s, is much larger for the same $\Lambda_{div,near}$ or $\Lambda_{div,far}$. *Neither $\Lambda_{div,near}$ nor $\Lambda_{div,far}$ are good predictors of upstream shoulder formation or growth.*

To further demonstrate the lack of effect of divertor N level on the upstream SOL density profile, we compare, from the same pulse (JPN90697), periods *prior* to N_2 seeding (early part of pulse) to periods *during* the seeding (latter part of pulse). First, we find that the pre-N injection trajectory of A_s vs $\Lambda_{div,near}$ (blue squares, 'pre-N_2 seed') follows the typical trajectory of unseeded discharges as described in section 4.1 (figure 7). As the N_2 seeding is added (gold triangles, 'during N_2 seeding' later in the same discharge) the data shift to larger $\Lambda_{div,near}$ while the shoulder amplitude, A_s, drops slightly (gold triangles). In contrast, $\Lambda_{div,far}$ shows almost no change with N_2 seeding.

Legacy N adsorbed on vessel surfaces, as reported in [55], can strongly affect the divertor condition and SOL density shoulder in the following pulse. Figure 14 also displays the results

(green triangles) from the early part of pulse (JPN90700) before N_2 seeding starts; however, the previous pulse had strong N_2 seeding and thus there is a large amount of N adsorbed on the vessel surfaces. Our only indirect measure of N in the divertor plasma is an NII emission line, the brightness of which is approximately the same for the early part of this pulse (JPN90700) as during the period of HR conditions during N_2 seeding in a previous pulse (JPN90697, same figure).

The 'N loaded' discharge (JPN90700) data follows a trajectory in (A_s vs Λ_{div}) space that is different than pulse JPN90697 and the D_2 fuelled pulses using the HT of section 4.1. In both the near and far SOL, Λ_{div} increases to or above 10 before A_s begins to increase. Figure 14 (a) and (b) thus demonstrates *that there is no general relationship between* Λ_{div}, with A_s *in either the near or far SOL*; parallel resistivity is not the sole mechanism affecting shoulder growth. We now turn our attention to other mechanisms described in the introduction.

5. Main chamber SOL ionization

In this section, we present evidence that suggests local ionization in the main chamber SOL does not strongly influence the shoulder formation. Figure 15 displays a comparison of two (D_2 fuelled) density ramp pulses, one each utilizing the HT and VT configurations, plotted with solid and dash-dot lines, respectively. Normalized density profiles (a), and ionization rate profiles (b), are shown for the three $\overline{n}_e$ selected at the times corresponding to the vertical lines in (c), which displays the midplane neutral pressure (Penning gauges). Separatrix densities were also equal for each divertor target configuration and $\overline{n}_e$.

Despite the lack of shoulder, the local neutral ionization rate, S_{ion}, is of greater magnitude in the VT for all $\overline{n}_e$. Further, the shape of the S_{ion} profile in the HT is broader where a shoulder is present. This indicates that the shape of the ionisation profile is more determined by the n_e profile, rather than vice versa.

Additionally, the mid-plane pressure, measured by Penning gauges, shows an equivalent functional dependence on $\overline{n}_e$ for both target configurations (figure 15 (c)). This indicates that the magnitude of the flux of neutrals toward the plasma cannot be solely responsible for setting the profile shape, consistent with the ionization profile shown in (b); the broadened S_{ion} profiles for the HT are due to the increased density in the far SOL rather than an increased influx of neurtals.

These results indicate that, like Λ_{div}, the ionisation of midplane neutrals (shoulder formation mechanism c) is not sufficient to flatten the density profile and that there must be some other

mechanism which influences the shoulder formation. Given that separatrix densities and core conditions were equivalent for each divertor target configuration and $\overline{n}_e$, potential shoulder mechanism a) is unlikely to be a determining factor in shoulder formation unless turbulence at the separatrix changes with divertor configuration.

6. Divertor neutral processes

Divertor neutral processes could be reducing the loss of ions out of the upstream SOL – the so-called ion 'sink' or drainage mechanism for upstream shoulder formation (shoulder formation mechanism d), outlined in the Introduction. Our primary measure of neutral processes in the divertor is through the intensity and distribution of D_α, which can be roughly related to the distribution of both ionization and charge exchange (CX). The connection between those processes and parallel flows will be discussed in more detail in the Discussion section.

The ionization rate, $S_{ion} = n_e n_0 \langle \sigma v \rangle_{ioniz}$ is dependent on n_0, the neutral density, and $\langle \sigma v \rangle_{ioniz,}$ the electron ionization rate coefficient. S_{ion} has a similar functional dependence on temperature as the D_α emission rate for temperatures of 10eV and above (dominated by excitation in attached plasmas). The result is that the number of ionizations per emitted D_α photon does not vary much in this range (but does not take into account ionizations occurring through molecules, roughly a factor of 2 effect). Therefore divertor D_α is a good proxy, in a relative sense, for divertor ionization in this temperature range. Between 10 eV and 5 eV, or potentially lower, the number of ionizations per D_α photon drops by a factor of ~ 2.

The divertor D_α emission region is also a good proxy for the extent as well as the number of CX reactions occurring in the divertor ($S_{CX} = n_i n_0 \langle \sigma v \rangle_{CX}$). Both the charge exchange and D_α excitation rates are, again, fairly constant above 10 eV. For T_e below 10eV, the number of charge exchange events per D_α photon increases since the D_α excitation rate is dropping.

As described in Section 2, we monitor the divertor D_α by both chordal spectroscopy measurements of D_α through the divertor cross-section, as well as toroidally-viewing camera images of the divertor region, filtered for D_α, which are tomographically inverted to provide a 2D pattern of D_α emissivity (photons/(m^3s)).

6.1 Strike point sweeping and effect on upstream density shoulders

Through minimal radial sweeping of the strike point across the HT (total target distance of 5 cm) we find that the changes in the total D_α emission integrated across the divertor (I-D_α, the sum of multiple chordal D_α brightnesses across the outer divertor) also oscillates in the same sawtooth

fashion as the strike point location, $R_{strikepoint}$ (figure 16 (a)). The close correlation between movement of the strike point, A_s, and I-D_α, is shown in figure 16 versus time.

Following the formation of a small shoulder (figure 16 b, 8.5s) with core density rise due to initial high D_2 fuelling rate, both A_s (16 b) and I-D_α (16 c) oscillate in anti-phase with respect to the radius of the outer strike point, R_{sp} (figure 16 c). In other words, I-D_α (and A_s) are both maximized when R_{sp} is smallest - when the strike point is farthest from the entrance to the pump and thus fewer neutrals are being removed.

Figure 17 displays the correlation between the different characteristics given in figure 16. The strong correlation between A_s and I-D_α (b) as well as between I-D_α and R_{sp} (a) quantitatively reflect what is evident from figure 16; small changes in the divertor D_α (and thus ionization and charge exchange) correlate with observable changes in A_s upstream. In contrast, Λ_{div}, within error bars, does not change with A_s (figure 17 c and d);

We have also investigated the cross-correlation time delay between A_s and R_{sp} as well as A_s and I-D_α. The cross-correlation time for the latter two variables is ~0 within the time resolution of A_s (10 ms). This is consistent with changes in the divertor I-D_α, representative of neutral processes, directly leading to changes in the upstream density profile.

The most important observation is that strike point sweeping leads to a modulation of the shoulder amplitude, while the upstream and divertor density and Λ_{div} remain constant, or do not change outside of uncertainties. Strike point sweeping was also present during the D_2 fuelling ramps described earlier in section 4, which focused on the HT, but no amplitude modulation was observed, suggesting that the amplitude modulation is only present below a certain fuelling rate and for small shoulders. Nevertheless, the effect of the strike point sweeping indicates that there is some other mechanism, likely related to divertor neutral processes, that influences upstream radial transport.

6.2 Comparison of VT and HT D_α emissivity profiles

Another test of whether divertor D_α, and thus divertor neutral processes, are affecting upstream density shoulder profiles is to explore that connection for changes in divertor geometry through examination of figure 18. We utilize the D_α emissivities derived from KL11 camera D_α camera inversions given the vertical chordal measurements used in I-D_α do not properly cover the vertical target. The contour plots of D_α emissivity are shown for three core densities for both the HT and VT geometries. Flux surfaces are dotted and are separated in normalized flux Ψ by 0.01 (Ψ_{sep} =1). The uncertainty in the location of D_α contours is of order 2-3cm and is due to uncertainties in mapping optical camera pixels to vessel structures and in equilibrium reconstruction.

Examining the first column (figure 18 a and d), when the divertor is in the SL regime, only slight differences in the D_α magnitude and extent are found between HT and VT configurations. The slight shift of the VT D_α emissivity region into the private flux region is within uncertainties in EFIT as well as the unknown amount of reflections. However, the shift could also be due to the divertor geometry; recycled neutrals from a HT would mostly travel towards the common flux region while, for the VT, recycled neutrals move towards the private flux region. Such directional differences in recycled neutrals would be consistent with higher measured sub-divertor pressures for the VT compared to the HT for a given $\overline{n}_e$.

The difference in D_α emissivity between HT and VT operation becomes pronounced as the shoulder is formed. Figure 18 (b and e) correspond to a later phase in the same pulse where both configurations have transitioned to HR divertor conditions (just in the near SOL for the VT). The upstream SOL density shoulder has formed in the HT, but not in the VT. Firstly, the peak emissivity in the HT configuration is ~ 2x higher than for the VT. Secondly, there is a clear difference in the shape of the emission region, the equivalent contour line (e.g. red) for the HT extends over a wider region (x2) towards the common flux region of SOL, than for the VT.

As the core density is increased further (figure 18 c and f), the shoulder amplitude saturates for the HT, which is still in a high-recycling condition. The D_α emission region shape and maximum D_α emissivity remain relatively unchanged for the VT. On the other hand, the region of high D_α emissivity for the HT configuration continues to spread across and along flux surfaces and apparently also to larger R, spreading over the edge of the HT (R>2.82m).

6.3 The effect of N_2 seeding on divertor D_α profiles and magnitude.

It was shown in section 4.3 that N_2 seeding causes Λ_{div} to rise strongly without a corresponding increase in the upstream SOL density shoulder. In contrast to D_2 fuelling, N_2 seeding acts to reduce the divertor D_α emission, consistent with the lack of increase in upstream density shoulder amplitude.

This behavior is demonstrated in Figure 19, which shows traces from a later phase in the pulse discussed in section 6.1 (JPN90697). The increasing amount of N in the divertor, indicated by the NII brightness (a), is concurrent with the reduction in A_s (strike point sweep is causing A_s to oscillate). Traces C3-C7 show vertically viewing chordal measurements through the HT region (see figure 2 for chord locations) of D_α brightness from x-point major radius (C3 view) to R slightly greater than $R_{strikepoint}$ (C7 view). At low levels of NII brightness, the oscillation in D_α is visible on all channels. Increasing levels of N in the divertor correspond to drops in the D_α brightness of chords C5-C7 as well as brightness oscillation. The decreases in brightness occur

initially for the largest R channels (C6 and C7), moving progressively inwards in major radius to C4. As the D_α emission region shrinks toward the separatrix, A_s decreases; even if the divertor T_e is constant during the seeding ramp the amount of ionization and charge exchange events is likely decreasing – even more reductions should occur if the divertor T_e is dropping. The sub-divertor neutral pressure (not shown) remains constant over this time range.

Unlike $\Lambda_{div,}$ I-D_α is well-correlated with shoulder formation regardless of whether N is present in the discharge or not. Positive correlation is observed between A_s and I-D_α as was found for figures 16 and 17 where Λ_{div} was essentially not varied. This behavior is again demonstrated in Figure 20. The data from JPN90697 (blue squares) includes a density ramp to achieve a small shoulder, followed by a sweep of the strike point. During the density ramp period, there is a clear overlap with the trajectory of a standard density ramp of section 4.1 (JPN89346 black circles). Once the sweep starts, there is deviation from the case of only D_2 fuelling, consistent with only varying I-D_α as opposed to Λ_{div} (see section 6.1). Note that core density and Λ_{div} are held constant during the sweep as shown in Figure 17.

The third discharge included in figure 20 includes another layer of difference – namely the level of N still in the machine from previous pulses, 'N-loading'. This discharge (green triangles JPN90700) was previously used (figure 14) to demonstrate how Λ_{div} was a poor measure of shoulder amplitude, A_s. Here, we first find during the density ramp that I-D_α follows the unseeded HT cases (black circles, blue squares). This is followed by a period of strike point sweeping where, similar to the case of blue squares (formation of shoulder and then fuelling held constant during strike point sweeping) I-D_α increases and decreases as the strike point is moved away and towards the pump opening; A_s responds as in the case without N_2 seeding.

In all the cases shown in figure 20, with N_2 seeding or without, with sweeping or without, I-$D_{\alpha,}$ unlike Λ_{div}, correlates well with A_s.

7. Shoulder formation behavior in H-mode

While the research focus of the previous sections of this paper focus on L-mode plasmas, we have studied a few H-mode discharges where the ELM frequency was low enough to make measurements between ELMs. ELMs are major perturbations on the SOL and divertor plasma, where plasma characteristics are strongly varying within the measurement time resolution. The H-mode plasmas we show correspond to the outer strike point on the HT. Ramps in fuelling and nitrogen seeding were available and thus are easily compared to the equivalent L-mode discharges. In general, the behavior in H-modes was similar to that of a comparable L-mode.

7.1 H-mode D_2 fuelling ramp

The first case we address is the simplest of the previous sections, in which shoulders are also most evident – a D_2 fuelling ramp, which moves the divertor condition from sheath-limited through high-recycling. Figure 21 displays the time dependence of several core and divertor plasma parameters. Despite the factor of 8 increase in D_2 fuelling rate, there was little change to $\overline{n}_e$. However, the time averaged Γ_{div} (integral of ion current over the outer divertor) increased somewhat with increasing D_2 fuelling rate. The D_2 gas was injected through GIMs 10 and 11, figure 1, different from the L-mode cases. In the course of the fueling ramp, the ELM frequency increased from 25 to 100Hz. Vertical shaded bars with corresponding symbols indicate periods where the divertor and SOL data has been analyzed; the width of the shaded regions corresponds to the length of time over which data is averaged in the following description.

ELMs increase the density in the SOL rather than change the time-averaged profile shape. The SOL density profile 'between ELMs', shown in figure 22, is created by averaging profiles obtained during multiple inter-ELM periods during the shaded period (yellow) around 52.5s in figure 21. The profile labeled 'including ELMs' is averaged over multiple Li-beam measurement periods, but for frames including ELMs. The relatively weak increase in the normalized density of profiles which include ELMs is due to the exposure time of the Li beam being 2-3 times longer than the duration of the ELM.

The evolution of the divertor profiles of n_e, T_e and Λ_{div} during an H-mode fuelling scan shows little difference to L-mode HT plasmas. The profiles with different symbols/colors shown in figure 23 correspond to the color shaded regions of figure 21. All profiles correspond to inter-ELM periods. In the L-mode phase (blue squares) the divertor n_e (b) and T_e (d) profiles indicate slightly high-recycling conditions and a small upstream density shoulder. Upon transitioning to H-mode (green triangles), the density profile in both the near and the far SOL becomes steeper, consistent with the H-mode reduction in radial particle and energy transport. Simultaneously, the divertor target n_e reduces, and T_e increases strongly (leading to Λ_{div} decreasing), despite a significant increase (>2) in the separatrix density (not shown). Therefore, in transitioning from L-mode to H-mode, the divertor has also transitioned from HR to SL conditions and the small shoulder disappears; thus the L-mode relationship between the upstream density profiles and target conditions holds across the L-H mode transition for the case of HT D_2 fuelling ramp).

With increasing gas fueling, the divertor becomes more high recycling (red circles to black diamonds) and the corresponding Λ_{div} increases. Similar to the L-mode discharges of section 4.1,

a density shoulder forms in the upstream SOL beyond 1.5cm from the separatrix. With further increases in the D fueling rate, the shoulder amplitude and the density at the limiter radius substantially increase, and it appears that the shoulder moves inwards (broadening) which would mean that the near SOL region contracts by ~0.5cm (red circles to black diamonds). Detachment did not occur, even for the latest time point.

7.2 **H-mode N_2 seeding ramp**

As for the L-mode case (sections 4.3 & 6.3), divertor N_2 seeding does not lead to further flattening of the upstream density profile. Figure 24 displays time traces for an N_2 seeding ramp where vertical shaded regions (time window of averaging inter-ELM periods) and symbols correspond to the profiles shown in figure 25. D_2 fuelling was held constant during the N_2 seeding rate ramp. We note that the ELM frequency was substantially lower than for the D_2 fuelling ramp case of figure 21, as has been previously observed [56].

The density profiles (Figure 25a) at the lowest Λ_{div} already shows substantial flattening and therefore any inferred value of A_s (Figure 25c) cannot be directly compared to the L-mode cases. For this reason, we do not interpret the profiles in the same manner as previous sections.

As in the D_2 fuelled case, during the transition to H-mode (green triangles) the density profile steepens generally. The divertor conditions are sheath-limited, indicated by high T_e. Further into the development of the H-mode, with increased $\overline{n}_e$ (red circles), the density profile in the far SOL is essentially the same as the L-mode. The near SOL, however, does differ with larger $n_{e,sep}$ and gradients in the H-mode. The

The subsequent rise in N_2 seeding does not modify the upstream density profile outside of uncertainties, yet there are strong changes to the divertor conditions and also Λ_{div}. Divertor densities peak (black stars) reduce by an order of magnitude (cyan pentagons). In this most detached case, $\overline{n}_e$ and $n_{e,sep}$, are higher and yet there is no appreciable increase in the far SOL density. The only significant change appears in the near SOL where the gradient increases.

As shown in figure 25 (c), Λ_{div} reaches a maximum just prior to the onset of detachment. The collisionality will continue to increase as detachment occurs. From this follow two important implications. Firstly that the dynamic range of Λ_{div}, when using target Langmuir probes, does not extend into detached conditions. Secondly, *and most crucially, strong increases in collisionality,*

beyond what is measureable by Λ_{div}, do not necessarily lead to further flattening of the density profile and thus enhanced main chamber radial fluxes, whether in L-mode or H-mode.

8. Discussion

The purpose of this study was to investigate possible mechanisms that control SOL density shoulder formation. As discussed in the introduction these include changes in filament birth characteristics together with changes in filament properties as it travels through the SOL: electrical effects (resistivity) on filament properties, local sources and sinks for ions. Here we review and discuss the various mechanisms studied in this paper.

8.1 The role of upstream conditions in shoulder formation

The results contained herein indicate that varying the divertor configuration brings a new tool to investigating the physics leading to SOL density shoulders. Under the same separatrix conditions and midplane neutral densities, SOL density shoulders appear for HT, but not for VT operation (section 5). Such results indicate that it is unlikely that separatrix filament generation (shoulder formation mechanism a) or fuelling of the upstream SOL (shoulder mechanism c) are significant contributing mechanisms to the shoulder formation.

We note that there is no clear agreement across the tokamak research community as to whether SOL ionization is raising the density in the SOL. An experimental study of shoulder formation on MAST [18] also found no correlation between a radial D_α chord measurement at the plasma mid-plane, associated with ionization, and changes to the profile flatness. The authors of [29] pointed out that if there was enough local ionization to affect the density profile then the local T_e should drop as the ionization energy is an energy loss and new ions (coming from cold neutrals) will have lower plasma temperatures – this is not observed in that study or at C-Mod [57]. In addition, modelling of the SOL by Stangeby concluded that local ionization is likely not a strong effect [58].

There are several cases where authors [19, 45] felt that when the mean free path for ionization of neutrals and charge exchange, $\lambda_{iz,cx}$, is small compared the thickness of the SOL –a so-called radial high recycling condition ensues; ionization raises the local density leading to more ionization and further density rise. Ultimately, however, increased SOL densities due to shoulder formation will always lead to more ionization in the SOL, but this is not necessarily evidence of a positive feedback loop and the existence of the radial high-recycling condition. Indeed the results presented in this paper have decoupled the increased SOL ionization and the formation of the shoulder.

We have noted that after the SOL density shoulder completely forms, a second phase follows,

correlating with detachment for the HT; the shoulder extends/expands towards the limiter. Ionization could be contributing to this expansion of the shoulder to larger R, but we cannot comment on that contribution relative to other mechanisms. .

What is clear is that it would be useful to produce more detailed studies of the profile of the ionization source rate across the SOL, its correlation with shoulder formation/expansion and comparison to estimates of parallel losses.

8.2 Parallel resistivity

There is broader agreement between our study and those on TCV and ASDEX-Upgrade [37, 45] that increases in parallel resistivity ($\Lambda_{div} > 1$) are *not* a 'sufficient' condition for SOL density formation. For Vianello [37], this conclusion came from a set of discharges where $\Lambda_{div} >> 1$ (near or far) and yet, in some cases SOL density shoulders occurred, and in other discharges shoulders did not. In the case of our JET L-mode studies we reach the same conclusion but through a different test, N_2 seeding.

ASDEX-Upgrade N_2 seeded, L-mode, vertical target discharges [36] are somewhat at odds with our JET results; Both D_2 fuelling or N_2 seeding raise divertor collisionality (Λ_{div}) and lead to shoulder formation (They say 'These results are independent on how *detachment* is achieved'). On the other hand, the more recent ASDEX-Upgrade study of H-mode plasmas [45] indicates that N_2 seeding, without significant D_2 fuelling, did not lead to lead to SOL density shoulder formation even though $\Lambda_{div} >> 1$.

8.3 Divertor neutral processes

The insufficiency of Λ_{div} in controlling the shoulder properties led to the search for an alternative mechanism. Based on the results presented in section 6, we speculate that 'recycling' or 'neutral processes' in the divertor modify flows out of the SOL.

The divertor D_α emissivity, integrated over the outer divertor region, I-D_α, correlates well to upstream density shoulder amplitude: a) It does not rise as N_2 seeding is used to make the divertor more recycling and Λ_{div} increases; b) Sweeping of the outer strike point back and forth across the HT strongly affects I-D_α in direct correlation with shoulder amplitude upstream (and immediately, within the time resolution of the diagnostic); and c) switching from HT (shoulder) to VT (small, or no shoulder) geometry lowers I-D_α and A_s and shrinks the region of high D_α emission away from the far SOL, the location of the upstream density shoulder.

The strike point sweep data has a subtle implication for the control of the upstream density shoulder. During strike point sweeps the divertor target surface measures of n_e and T_e, and thus

Λ_{div}, did not measurably vary. And yet small changes in I-D_α, which is indicative of ion-neutral interactions near the target, correlate with changes in upstream A_s.

All of the above correlations of I-D_α with A_s, indicate that I-D_α is a more consistent indicator of shoulder changes than Λ_{div}. But a more detailed study is needed, along with modeling, to better understand the roles of underlying processes.

EDGE2D-EIRENE modelling of unseeded H-mode plasmas with VT and HT [59] shows a strong similarity to the experimental results presented here. The modeled divertor ionization distribution at the target is much broader in HT compared to the VT configuration. The density across the entire SOL was increased for HT compared to VT, although the profile shape was generally the same. The lack of a localized effect in the region of the upstream density shoulder may not be surprising given such fluid codes do not take into account cross-field transport due to turbulence or even convection.

There is a significant literature base from divertor fluid models and experimental measurements that supports the connection between increased divertor ionization leading to lower flows into the divertor – a mechanism that can reduce the loss of ions, or their 'drainage' from the upstream SOL and thus increase the upstream density (shoulder formation mechanism d). Ionization in the divertor plasma has been shown in multiple models (fluid and analytic) to affect flow magnitude and direction, even leading to 'reverse flows' out of the divertor towards the SOL[60-64]. Variations in flows can be localized and thus could affect just to regions of the divertor which could then correspond to the upstream SOL shoulder region. In addition, we also know that charge exchange processes can directly lead to reduced flows in the divertor as well through momentum removal (particularly detachment). The authors of [29] even argued, independent of detachment, that 'the CX induced friction with the neutrals over the entire flux tube slows down the plasma motion towards the target hence "clogging" its flow out of the SOL.

A recent model by Walkden [65] relating SOL filaments and shoulder formation also pointed towards reduced flows out of the SOL as an important mechanism for SOL density shoulder formation. The model compares parallel resistivity, upstream ionization and drainage as mechanisms for shoulder formation. Increased ionization, as a source for ions, cannot be differentiated in that model from a decrease in ion drainage so they should be viewed as the same for that study. It was found that localized source/sink changes are the optimal mechanism to create localized shoulders compared to changes in local parallel resistivity.

There are also direct measurements of parallel flow in the upstream SOL that do not support the reduction of flows with increasing density. Lipschultz's summarization of measurements of the parallel flow velocity profile over several tokamaks [19], indicate that parallel flows toward the

divertor *increase* with increasing density in the near SOL of JET and C-Mod. Hidalgo et al's measurements of turbulence characteristics on JET [66] led to the statement that 'as the size of transport events increases, parallel flows also increase'; this would indicate that as parallel resistivity increased, and thus increases in filament size, parallel ion losses would *increase* instead of *decrease* as required to increase the SOL density.

We have no direct proof that divertor neutral processes are leading to shoulder formation through reductions in parallel flows out of the upstream SOL. However, the changes in I-D_α are the most consistent with changes in the SOL density shoulder motivating more investigation of the relation between plasma-neutral processes in the divertor and main chamber radial transport.

8.4 Shoulders and H-mode plasmas

Evidence of density shoulders in the SOL of H-mode plasmas is relatively sparse in the literature. To the best of our knowledge, this paper presents the first measurements of shoulders in H-mode plasmas on JET-ILW. N_2 seeding led to even higher values of collisionality than L-mode, and yet changes to the SOL density profile were *still* not observed. This adds to the strong evidence against Λ_{div} as a sufficient control parameter, and also of the more general filament electrical disconnection hypothesis that has been widely used to explain the enhancement of radial fluxes [25, 31, 33, 36].

9.0 Summary

We have explored four mechanisms, outlined in the introduction, which could affect the formation of density shoulders in the far SOL. We find that the probability of upstream mechanisms being responsible for shoulder formation is low. SOL density shoulders form and expand for the case of discharges utilizing the HT while, for the same core/separatrix conditions (assuming filament birth characteristics held constant) and midplane neutral pressure (neutral influx and total ionization held constant), shoulders do not form when the VT is used. *If the upstream SOL density shoulder mechanisms were important then divertor configuration should not matter.*

Turning to the effect of parallel resistivity on the upstream SOL density profile (changing filament characteristics through changes in parallel resistivity) our conclusions are similar to those reached by Vianello [37] namely that increases in $\boldsymbol{\Lambda}_{div}$ *are not sufficient* to lead to shoulder formation. In difference to the Vianello study, this conclusion is based on HT geometry plasmas where D_2 fuelled, density ramp discharges are compared with N_2 seeded discharges at constant core density. While the D_2 fuelling leads to strong increases in $\boldsymbol{\Lambda}_{div}$ that correlate with increased shoulder

amplitude, the same variation in $\boldsymbol{\Lambda}_{div}$, driven by N_2 seeding, has essentially no effect (or even a negative effect) on upstream shoulder amplitude. *If the primary mechanism of shoulder formation depends on increases in parallel resistivity then D_2 fuelling and N_2 seeding to increase Λ_{div} should be equivalent.*

Our results do imply that changes in ion-neutral processes in the divertor, as measured through the distribution and magnitude of D_a, is more consistent with shoulder formation; such changes in D_α can be related to changes in parallel flows. Unlike for $\boldsymbol{\Lambda}_{div}$, the magnitude and spatial extent of divertor-integrated D_a emissivity magnitude (I-D_α) *do* increase with upstream shoulder amplitude under D_2 fuelling and *do not* increase with N_2 seeding (no shoulder). Under the same D_2 fuelled core conditions I-D_α increases with increased shoulder amplitude for operation utilizing the HT, but I-D_α and its spatial extent do not increase for VT discharges where no shoulders are formed. Finally, strike point sweeping showed that upstream shoulder amplitude varies with I-D_α; this is without changes in $\boldsymbol{\Lambda}_{div}$. Based on past research the ionization and charge exchange (D_α emissivity is a measure) ion-neutral processes are plausible processes that can reduce flows to the target, thus reducing the loss of ions out of the upstream SOL (either filaments of steady state plasmas), increasing the upstream density.

When the HT divertor is pushed into detachment with D_2 fuelling the upstream density shoulder amplitude stops increasing and there is a clear expansion of the shoulder region towards the limiter radius. Such behaviour may be due to local SOL ionization as the mean free path for ionization of neutrals in the SOL (launched from limiters or wall surfaces) shortens and the neutral influx increases.

We have briefly examined the SOL and divertor characteristics during the period between ELMs for H-mode discharges. Only two discharges were examined and, as expected, the e-folding length for density in the SOL without shoulders is shorter in H-mode compared to L-mode plasmas. The same differences between shoulder formation with D_2 fuelling and N_2 seeding found for L-mode plasmas transfer to H-mode.

10. Acknowledgements

The authors are grateful for discussions with N. Vianello and D. Carralero as this study progressed. This work has been carried out within the framework of the EUROfusion Consortium and has received funding from the Euratom research and training programme 2014-2018 under grant agreement No 633053. The views and opinions expressed herein do not necessarily reflect those of the European Commission. We also acknowledge support from the EPSRC grants

EP/L01663X/1 and EP/K504178/1, which fund the University of York, EPSRC-funded, Centre for Doctoral Training in the Science and Technology of Fusion Energy. The research by B. Lipschultz was funded in part by the Wolfson Foundation and UK Royal Society through a Royal Society Wolfson Research Merit Award as well as by the RCUK Energy Programme (EPSRC grant number EP/I501045).

References

[1] Pitts, R, Kukushkin, A, Loarte, A, Martin, A, Merola, M, Kessel, C, Komarov, V, et al., "Status and physics basis of the ITER divertor", Physica Scripta, **2009** (2009) 014001.
[2] Eich, T, Leonard, A, Pitts, R, Fundamenski, W, Goldston, R, Gray, T, Herrmann, A, et al., "Scaling of the tokamak near the scrape-off layer H-mode power width and implications for ITER", Nuclear fusion, **53** (2013) 093031.
[3] Stangeby, PC, The plasma boundary of magnetic fusion devices, Institute of Physics Publishing Bristol, 2000.
[4] Pitcher, CS, Stangeby, P, "Experimental divertor physics", Plasma Physics and Controlled Fusion, **39** (1997) 779.
[5] Lipschultz, B, Bonnin, X, Counsell, G, Kallenbach, A, Kukushkin, A, Krieger, K, Leonard, A, et al., "Plasma–surface interaction, scrape-off layer and divertor physics: implications for ITER", Nuclear Fusion, **47** (2007) 1189.
[6] Labombard, B, Goetz, J, Hutchinson, I, Jablonski, D, Kesner, J, Kurz, C, Lipschultz, B, et al., "Experimental investigation of transport phenomena in the scrape-off layer and divertor", Journal of Nuclear Materials, **241** (1997) 149.
[7] Labombard, B, Umansky, M, Boivin, R, Goetz, J, Hughes, J, Lipschultz, B, Mossessian, D, et al., "Cross-field plasma transport and main-chamber recycling in diverted plasmas on Alcator C-Mod", Nuclear Fusion, **40** (2000) 2041.
[8] Rudakov, D, Boedo, J, Moyer, R, Stangeby, PC, Watkins, J, Whyte, D, Zeng, L, et al., "Far SOL transport and main wall plasma interaction in DIII-D", Nuclear fusion, **45** (2005) 1589.
[9] Behrisch, R, Federici, G, Kukushkin, A, Reiter, D, "Material erosion at the vessel walls of future fusion devices", Journal of Nuclear Materials, **313** (2003) 388.
[10] Whyte, D, Lipschultz, B, Stangeby, P, Boedo, J, Rudakov, D, Watkins, J, West, W, "The magnitude of plasma flux to the main-wall in the DIII-D tokamak", Plasma physics and controlled fusion, **47** (2005) 1579.
[11] Brezinsek, S, Widdowson, A, Mayer, M, Philipps, V, Baron-Wiechec, P, Coenen, J, Heinola, K, et al., "Beryllium migration in JET ITER-like wall plasmas", Nuclear fusion, **55** (2015) 063021.
[12] Brezinsek, S, Loarer, T, Philipps, V, Esser, HG, Grünhagen, S, Smith, R, Felton, R, et al., "Fuel retention studies with the ITER-Like Wall in JET", Nuclear Fusion, **53** (2013) 083023.
[13] image inversion, https://git.ccfe.ac.uk/jrh/kl11
[14] Mccormick, K, Kyriakakis, G, Neuhauser, J, Kakoulidis, E, Schweinzer, J, Tsois, N, "Particle and energy transport scalings in the ASDEX scrape-off layer", Journal of nuclear materials, **196** (1992) 264.

[15] Garcia, O, Horacek, J, Pitts, R, Nielsen, A, Fundamenski, W, Graves, J, Naulin, V, et al., "Interchange turbulence in the TCV scrape-off layer", Plasma physics and controlled fusion, **48** (2005) L1.
[16] Carralero, D, Birkenmeier, G, Müller, H, Manz, P, Müller, S, Reimold, F, Stroth, U, et al., "An experimental investigation of the high density transition of the scrape-off layer transport in ASDEX Upgrade", Nuclear Fusion, **54** (2014) 123005.
[17] Carralero, D, Müller, H, Groth, M, Komm, M, Adamek, J, Birkenmeier, G, Brix, M, et al., "Implications of high density operation on SOL transport: a multimachine investigation", Journal of Nuclear Materials, **463** (2015) 123.
[18] Militello, F, Garzotti, L, Harrison, J, Omotani, J, Scannell, R, Allan, S, Kirk, A, et al., "Characterisation of the L-mode scrape off layer in MAST: decay lengths", Nuclear Fusion, **56** (2015) 016006.
[19] Lipschultz, B, Whyte, D, Labombard, B, "Comparison of particle transport in the scrape-off layer plasmas of Alcator C-Mod and DIII-D", Plasma Physics and Controlled Fusion, **47** (2005) 1559.
[20] Labombard, B, Boivin, R, Greenwald, M, Hughes, J, Lipschultz, B, Mossessian, D, Pitcher, C, et al., "Particle transport in the scrape-off layer and its relationship to discharge density limit in Alcator C-Mod", Physics of Plasmas, **8** (2001) 2107.
[21] Matthews, GF, Edwards, P, Hirai, T, Kear, M, Lioure, A, Lomas, P, Loving, A, et al., Overview of the ITER-like Wall Project in: 11th International Workshop on Plasma-Facing Materials and Components for Fusion Applications, Greifswald, Germany, 2006.
[22] Umansky, M, Krasheninnikov, S, Labombard, B, Terry, J, "Comments on particle and energy balance in the edge plasma of Alcator C-Mod", Physics of Plasmas, **5** (1998) 3373.
[23] Antar, G, Krasheninnikov, S, Devynck, P, Doerner, R, Hollmann, E, Boedo, J, Luckhardt, S, et al., "Experimental evidence of intermittent convection in the edge of magnetic confinement devices", Physical review letters, **87** (2001) 065001.
[24] Boedo, JA, Rudakov, D, Moyer, R, Krasheninnikov, S, Whyte, D, Mckee, G, Tynan, G, et al., "Transport by intermittent convection in the boundary of the DIII-D tokamak", Physics of Plasmas, **8** (2001) 4826.
[25] Garcia, OE, Pitts, R, Horacek, J, Madsen, J, Naulin, V, Nielsen, AH, Rasmussen, JJ, "Collisionality dependent transport in TCV SOL plasmas", Plasma Physics and Controlled Fusion, **49** (2007) B47.
[26] Militello, F, Tamain, P, Fundamenski, W, Kirk, A, Naulin, V, Nielsen, AH, "Experimental and numerical characterization of the turbulence in the scrape-off layer of MAST", Plasma Physics and Controlled Fusion, **55** (2013) 025005.
[27] Garcia, O, "Stochastic modeling of intermittent scrape-off layer plasma fluctuations", Physical review letters, **108** (2012) 265001.
[28] Militello, F, Omotani, J, "Scrape off layer profiles interpreted with filament dynamics", Nuclear Fusion, **56** (2016) 104004.
[29] Militello, F, Omotani, J, "On the relation between non-exponential scrape off layer profiles and the dynamics of filaments", Plasma Physics and Controlled Fusion, **58** (2016) 125004.
[30] Halpern, FD, Ricci, P, Jolliet, S, Loizu, J, Morales, J, Mosetto, A, Musil, F, et al., "The GBS code for tokamak scrape-off layer simulations", Journal of Computational Physics, **315** (2016) 388.
[31] Krasheninnikov, SI, "On scrape off layer plasma transport", Physics Letters A, **283** (2001) 368.
[32] Kirk, A, Thornton, A, Harrison, J, Militello, F, Walkden, N, Team, M, Team, EM, "L-mode filament characteristics on MAST as a function of plasma current measured using visible imaging", Plasma Physics and Controlled Fusion, **58** (2016) 085008.
[33] Krasheninnikov, S, D'ippolito, D, Myra, J, "Recent theoretical progress in understanding coherent structures in edge and SOL turbulence", Journal of Plasma Physics, **74** (2008) 679.

[34] Myra, J, D'ippolito, D, Stotler, D, Zweben, S, Leblanc, B, Menard, J, Maqueda, R, et al., "Blob birth and transport in the tokamak edge plasma: Analysis of imaging data", Physics of plasmas, **13** (2006) 092509.
[35] Myra, J, Russell, D, D'ippolito, D, "Collisionality and magnetic geometry effects on tokamak edge turbulent transport. I. A two-region model with application to blobs", Physics of plasmas, **13** (2006) 112502.
[36] Carralero, D, Manz, P, Aho-Mantila, L, Birkenmeier, G, Brix, M, Groth, M, Müller, H, et al., "Experimental validation of a filament transport model in turbulent magnetized plasmas", Physical review letters, **115** (2015) 215002.
[37] Vianello, N, Tsui, C, Theiler, C, Allan, S, Boedo, J, Labit, B, Reimerdes, H, et al., "On Filamentary Transport in the TCV Tokamak: Addressing the Role of the Parallel Connection Length", Nuclear Fusion, **accepted** (2017).
[38] Angus, JR, Umansky, MV, Krasheninnikov, SI, "Effect of Drift Waves on Plasma Blob Dynamics", Physical Review Letters, **108** (2012) 215002.
[39] Angus, JR, Krasheninnikov, SI, Umansky, MV, "Effects of parallel electron dynamics on plasma blob transport", Physics of Plasmas, **19** (2012) 082312.
[40] Walkden, NR, Dudson, BD, Fishpool, G, "Characterization of 3D filament dynamics in a MAST SOL flux tube geometry", Plasma Physics and Controlled Fusion, **55** (2013) 105005.
[41] Walkden, NR, Dudson, BD, Easy, L, Fishpool, G, Omotani, JT, "Numerical investigation of isolated filament motion in a realistic tokamak geometry", Nuclear Fusion, **55** (2015) 113022.
[42] Militello, F, Walkden, NR, Farley, T, Gracias, WA, Olsen, J, Riva, F, Easy, L, et al., "Multi-code analysis of scrape-off layer filament dynamics in MAST", Plasma Physics and Controlled Fusion, **58** (2016) 105002.
[43] Riva, F, Colin, C, Denis, J, Easy, L, Furno, I, Madsen, J, Militello, F, et al., "Blob dynamics in the TORPEX experiment: a multi-code validation", Plasma Physics and Controlled Fusion, **58** (2016) 044005.
[44] Wersal, C, Ricci, P, "A first-principles self-consistent model of plasma turbulence and kinetic neutral dynamics in the tokamak scrape-off layer", Nuclear Fusion, **55** (2015) 123014.
[45] Carralero, D, Madsen, J, Artene, S, Bernert, M, Birkenmeier, G, Eich, T, Fuchert, G, et al., "A study on the density shoulder formation in the SOL of H-mode plasmas", Nuclear Materials and Energy, (2016).
[46] Wynn, A, Lipschultz, B, Matthews, G, Tal, B, Militello, F, Walkden, N, Guillemaut, C, et al., Radial fluxes and den¬sity shoul¬der for¬ma¬tion in the scrape off layer of JET, in: 22nd International Conference on Plasma Surface Interaction in Controlled Fusion Devices, Rome, 2016, pp. P2.46.
[47] Brix, M, Dodt, D, Korotkov, A, Morgan, P, Dunai, D, Fischer, R, Meigs, A, et al., "Upgrade of the lithium beam diagnostic at JET", Review of Scientific Instruments, **81** (2010) 10D733.
[48] Huber, A, Brezinsek, S, Mertens, P, Schweer, B, Sergienko, G, Terra, A, Arnoux, G, et al., "Development of a mirror-based endoscope for divertor spectroscopy on JET with the new ITER-like wall (invited)", Review of Scientific Instruments, **83** (2012) 10D511.
[49] Silburn, S, Calcam, in, 2016.
[50] Atomic Data and Analysis Structure, http://open.adas.ac.uk/
[51] Horacek, J, Pitts, RA, Stangeby, PC, Batishchev, O, Loarte, A, "Predicted effects of parallel temperature gradients on the overestimation of TCV divertor target Langmuir probe Te measurements", Journal of Nuclear Materials, **313** (2003) 931.
[52] Lipschultz, B, Goetz, J, Hutchinson, I, Labombard, B, Mccracken, G, Takase, K, Terry, JL, et al., Variation of the divertor geometry in Alcator C-Mod, in: 14th Int. Conf. on Plasma Physics and Controlled Fusion Research, IAEA, Vienna (1997), Montreal, 1996.
[53] Lipschultz, B, Labombard, B, Terry, JL, Boswell, C, Hutchinson, IH, "Divertor physics research on Alcator C-Mod", Fusion Science and Technology, **51** (2007) 369.
[54] Loarte, A, "Effects of divertor geometry on tokamak plasmas", Plasma Physics & Controlled Fusion, **43** (2001).

[55] Oberkofler, M, Douai, D, Brezinsek, S, Coenen, JW, Dittmar, T, Drenik, A, Romanelli, SG, et al., "First nitrogen-seeding experiments in JET with the ITER-like Wall", Journal of Nuclear Materials, **438** (2013) S258.
[56] Giroud, C, Jachmich, S, Jacquet, P, Järvinen, A, Lerche, E, Rimini, F, Aho-Mantila, L, et al., "Progress at JET in integrating ITER-relevant core and edge plasmas within the constraints of an ITER-like wall", Plasma Physics and Controlled Fusion, **57** (2015) 035004.
[57] Lipschultz, B, Labombard, B, Pitcher, C, Boivin, R, "Investigation of the origin of neutrals in the main chamber of Alcator C-Mod", Plasma physics and controlled fusion, **44** (2002) 733.
[58] Stangeby, PC, "Modeling plasma contact with the main vessel walls of a divertor tokamak", Physics of Plasmas, **9** (2002) 3489.
[59] Jaervinen, AEU, Brezinsek, S, Giroud, C, Groth, M, Guillemaut, C, Belo, P, Brix, M, et al., "Impact of divertor geometry on radiative divertor performance in JET H-mode plasmas", Plasma Physics and Controlled Fusion, **58** (2016).
[60] Cooke, PIH, Prinja, AK, "An analytic model for flow reversal in divertor plasmas", Nuclear Fusion, **27** (1987) 1165.
[61] Asakura, N, "Understanding the SOL flow in L-mode plasma on divertor tokamaks, and its influence on the plasma transport", Journal of Nuclear Materials, **363** (2007) 41.
[62] Schneider, R, Bosch, HS, Coster, D, Fuchs, JC, Gafert, J, Haas, G, Herrmann, A, et al., "Role of divertor geometry on detachment in ASDEX Upgrade", Journal of Nuclear Materials, **266–269** (1999) 175.
[63] Boedo, JA, Porter, GD, Schaffer, MJ, Lehmer, R, Moyer, RA, Watkins, JG, Evans, TE, et al., "Flow reversal, convection, and modeling in the DIII-D divertor", Physics of Plasmas, **5** (1998) 4305.
[64] Schneider, R, Bonnin, X, Borrass, K, Coster, D, Kastelewicz, H, Reiter, D, Rozhansky, V, et al., "Plasma Edge Physics with B2-Eirene", Contributions to Plasma Physics, **46** (2006) 3.
[65] Walkden, NR, Wynn, A, Militello, F, Lipschultz, B, Matthews, G, Guillemaut, C, Harrison, J, et al., "Interpretation of scrape-off layer profile evolution and first-wall ion flux statistics on JET using a stochastic framework based on fillamentary motion", Plasma Physics and Controlled Fusion, **59** (2017) 085009.
[66] Hidalgo, C, Gonçalves, B, Silva, C, Pedrosa, M, Erents, K, Hron, M, Matthews, G, "Experimental investigation of dynamical coupling between turbulent transport and parallel flows in the JET plasma-boundary region", Physical review letters, **91** (2003) 065001.

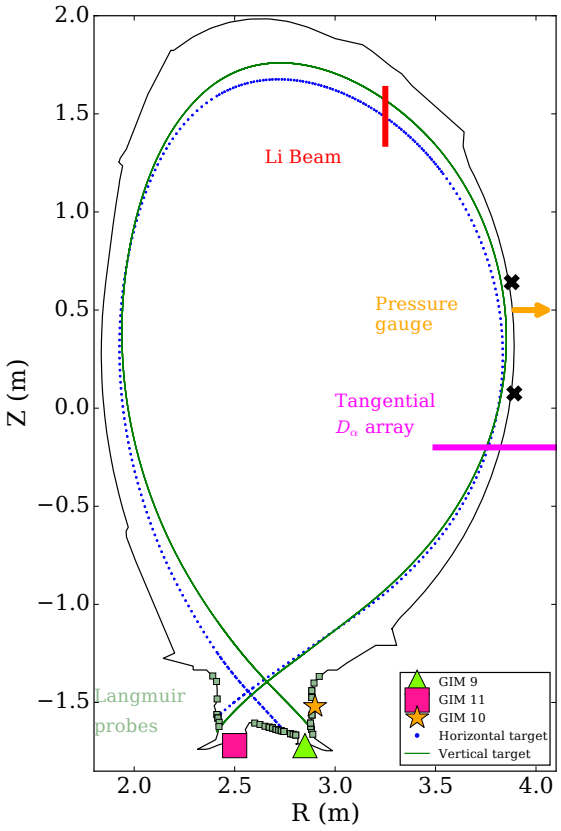

Figure 1: Diagnostics and gas injection module (GIMs) locations used in the study are shown with the magnetic equilibrium of the vertical and horizontal target divertor configurations.

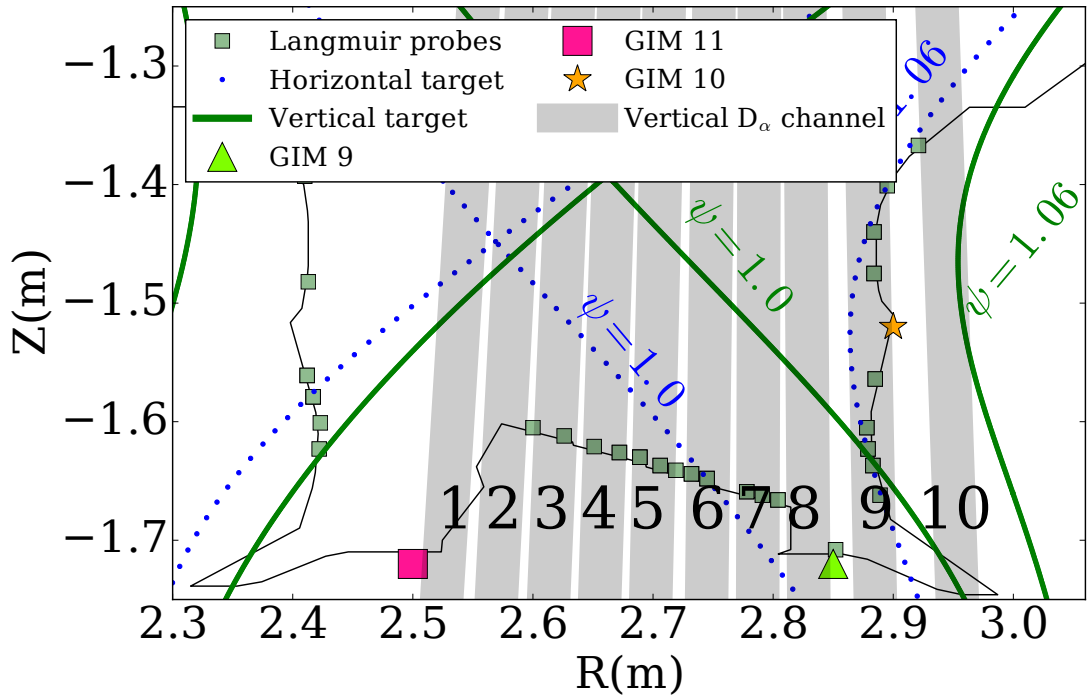

Figure 2: Close up of the divertor region showing the locations of the vertical viewing D_α channels (and other divertor diagnostics, not shown on figure 1.

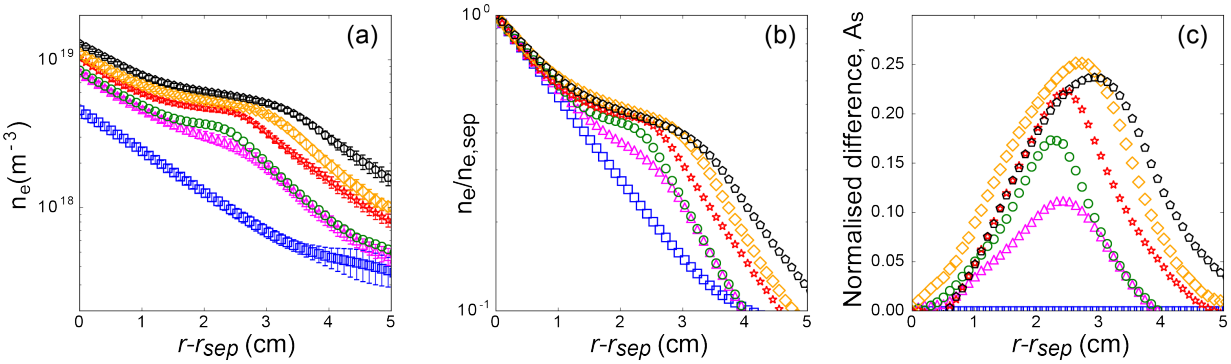

Figure 3: (a) Example density profiles during a horizontal target L-mode D fuelling ramp (JPN 89346) showing characteristic flattening. (b) The same density profiles normalised to separatrix density. (c) Normalised difference profiles calculated by subtracting the reference profile (blue squares) from a given profile.

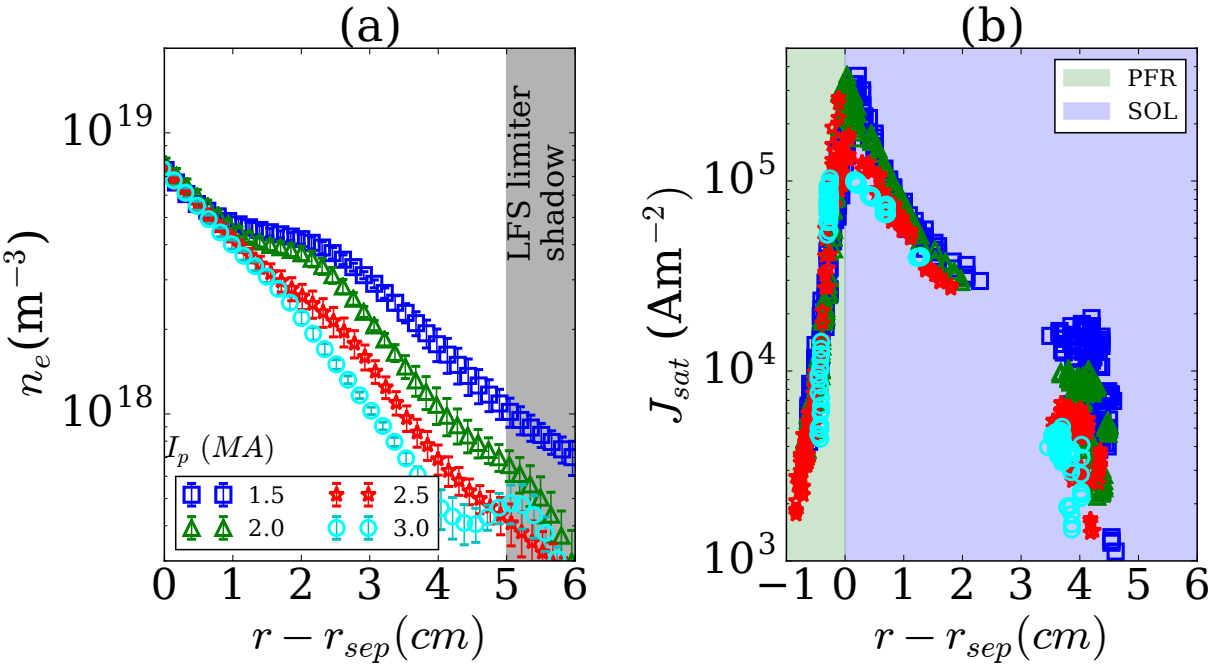

Figure 4: (a) Upstream density profiles for a fixed $\tilde{n}_e$ for a range of plasma current, I_p. (b) Corresponding change to the outer horizontal divertor J_{sat} profile. All profiles are mapped back to mid plane in terms of distance to the separatrix. The profiles shown are averaged over 10 measurement periods (100 ms). The error bars are the standard deviation of those measurements. The diagnostic signal to noise ratio near the limiter is of order 1 at the lowest densities and thus the deviation from the exponential is not significant. JPN893(44,50,46,48) ordered with increasing I_p.

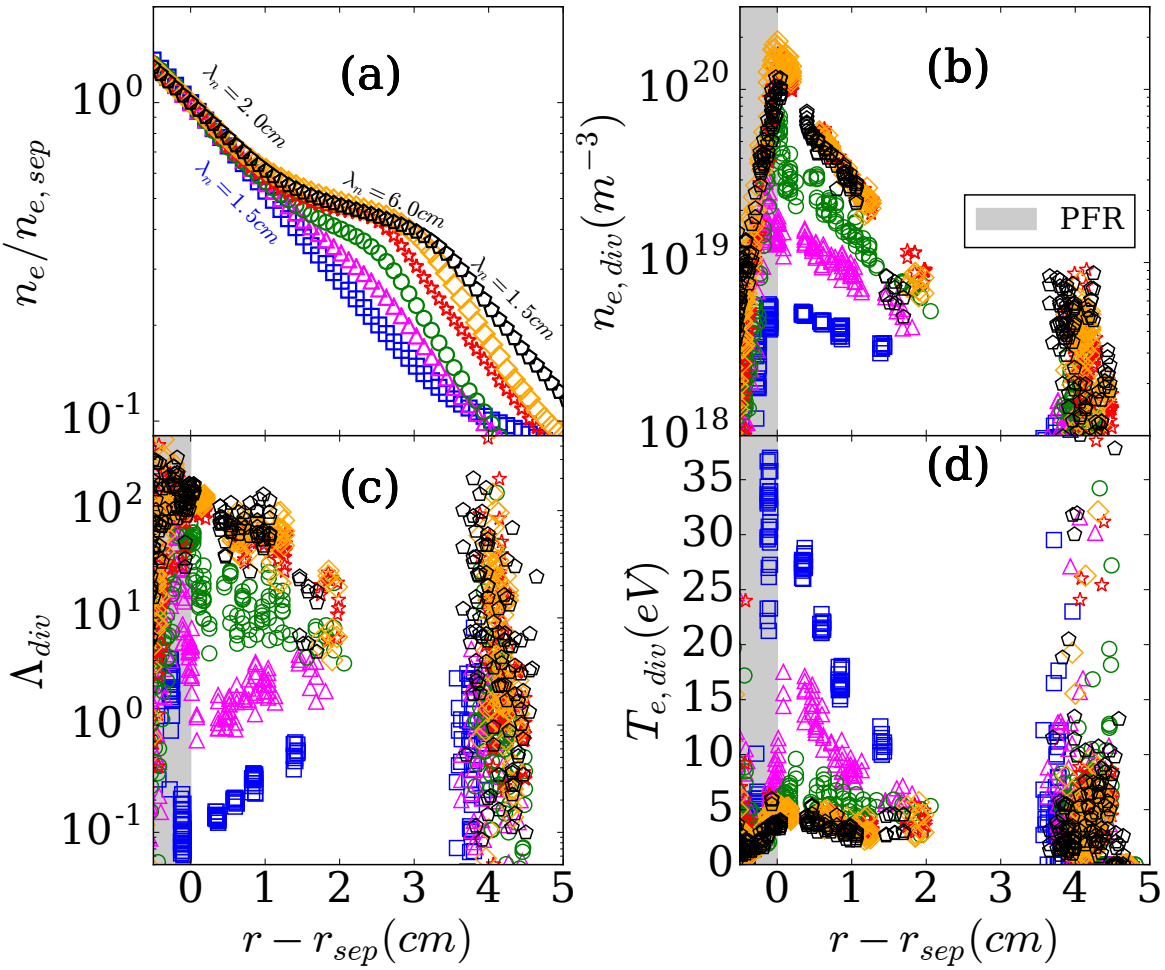

Figure 5: Horizontal target D fuelling ramp (JPN89346) for a 2.5MA plasma shown: (a) normalized SOL density profiles showing the formation and growth of the shoulder. (b) Divertor target density profiles showing the transition from SL (blue squares) to peak HR (red stars), as the divertor becomes more high-recycling (geen circles, red stars, orange diamnonds) and detachment onset (black pentagons) (c) The resultant change to $\mathbf{\Lambda}_{div}$; (d) Divertor T_e profiles. Limiter radius ~ r-r_{sep}~ 5 cm. Colour and symbols correspond to figure 6.

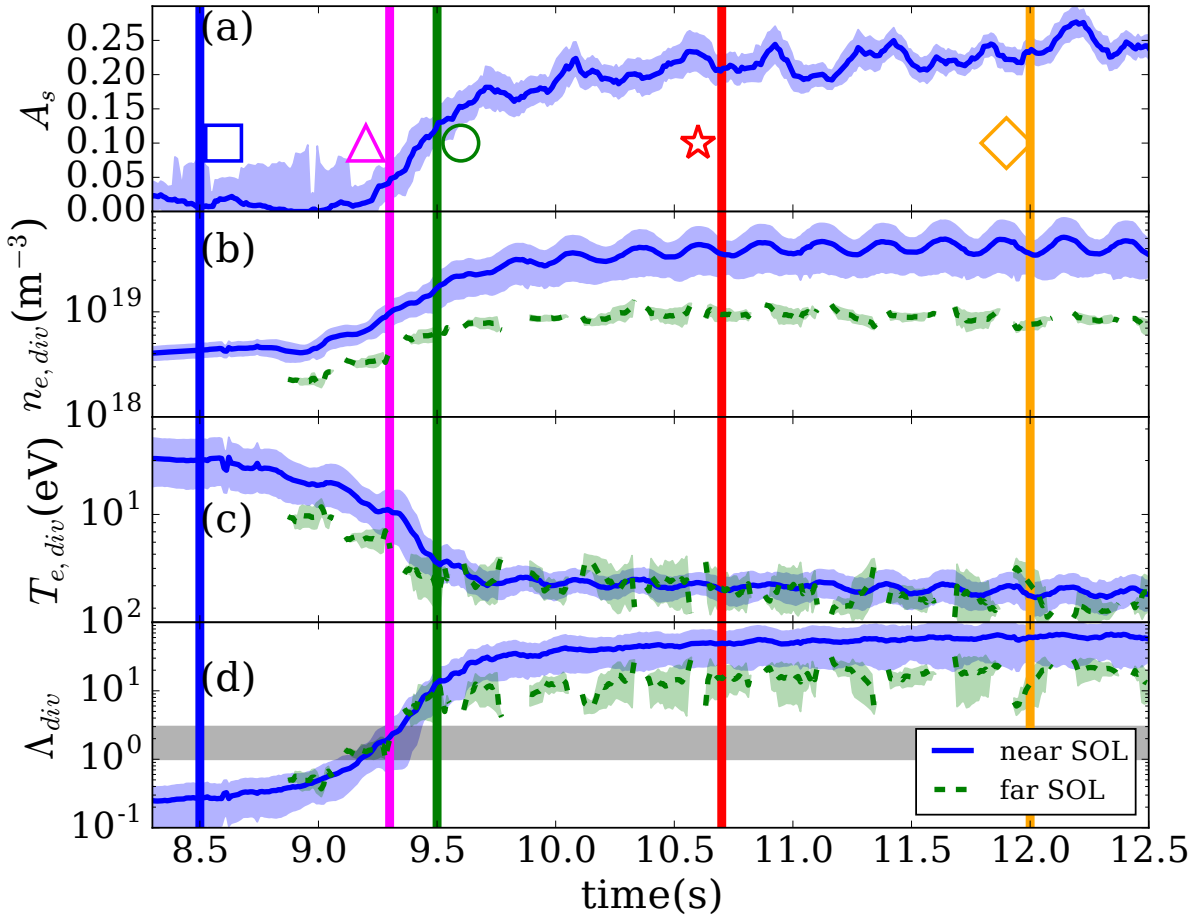

Figure 6: Time traces of quantities shown in figure 5 (JPN89346) with the same symbols and colors at times given by the vertical lines. The normalized shoulder amplitude, A_s is given in (a); (b) and (c) are the evolution of the density and temperature averaged over near ($r\text{-}r_{sep}$ = 0-1.5cm) and far ($r\text{-}r_{sep}$ = 1.5-3cm) SOL, referenced to the midplane; d) gives the divertor resistivities, $\Lambda_{div,near}$ and $\Lambda_{div,far}$, calculated using the data from (b) and (c). Gaps in data for far SOL are due to strike point sweeping and probe spacing.

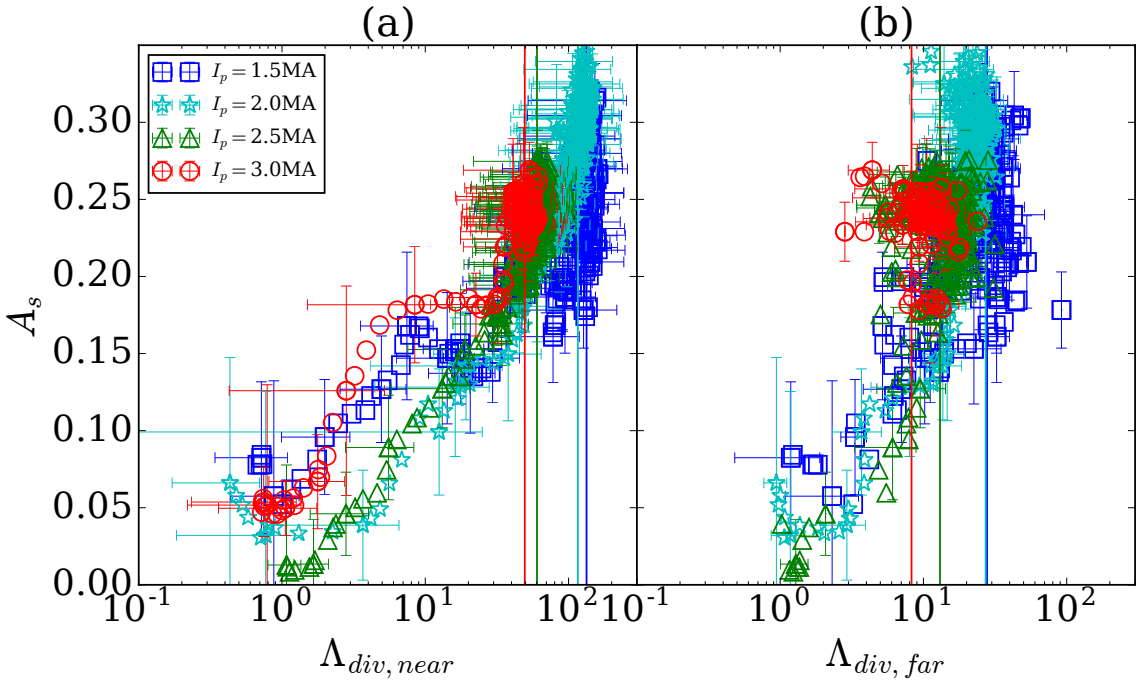

Figure 7: The shoulder amplitude, A_s, vs Λ_{div}, averaged over (a) near (r-rsep = 0-1.5cm) and (b) far (r-rsep = 1.5-3 cm) SOL regions for the 4 plasma currents of Fig. Ip_scan with L-mode, horizontal target plasmas, and D_2 puffing driving a core density ramp. Vertical lines indicate the onset of detachment for corresponding colours. The error bars are representative of the standard deviation of the data in the specified regions (near and far SOL) over 0.1s. JPN893(44,50,46,48) ordered with increasing I_p.

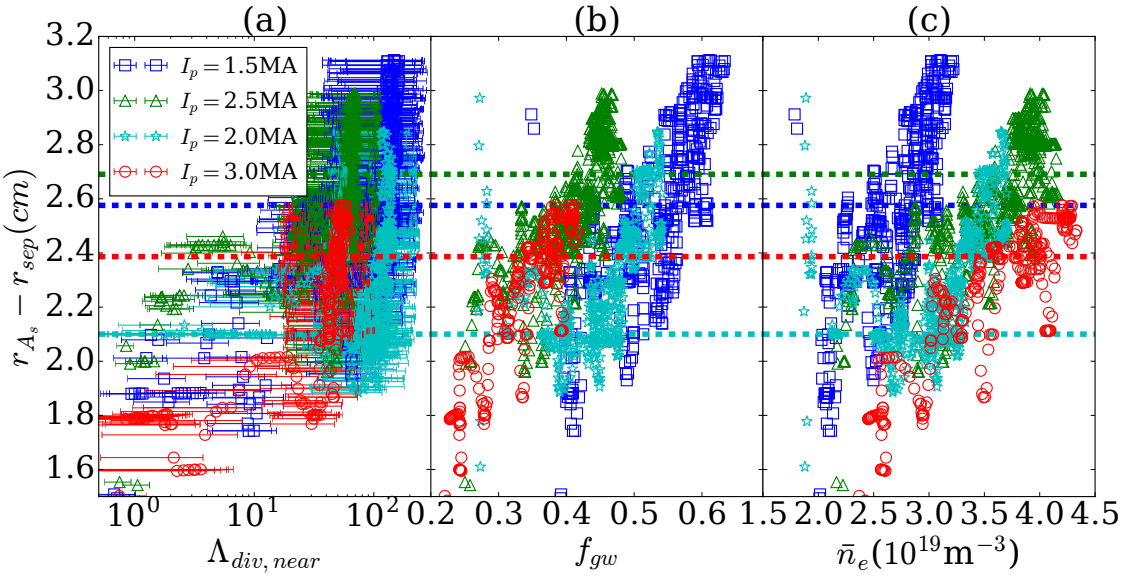

Figure 8: Movement of the radial location of A_s as a function of Λ_{div} (a) , $\tilde{n}_e/n_{gw}$ (b) and $\tilde{n}_e$ (c) for the 4 plasma currents of Fig. Ip_scan with L-mode, horizontal target plasmas and D_2 puffing driving a core density ramp. (a) Indicates the 2 phases of the profile evolution, initially formation and subsequent growth. Horizontal lines indicate the onset of detachment for each plasma current.

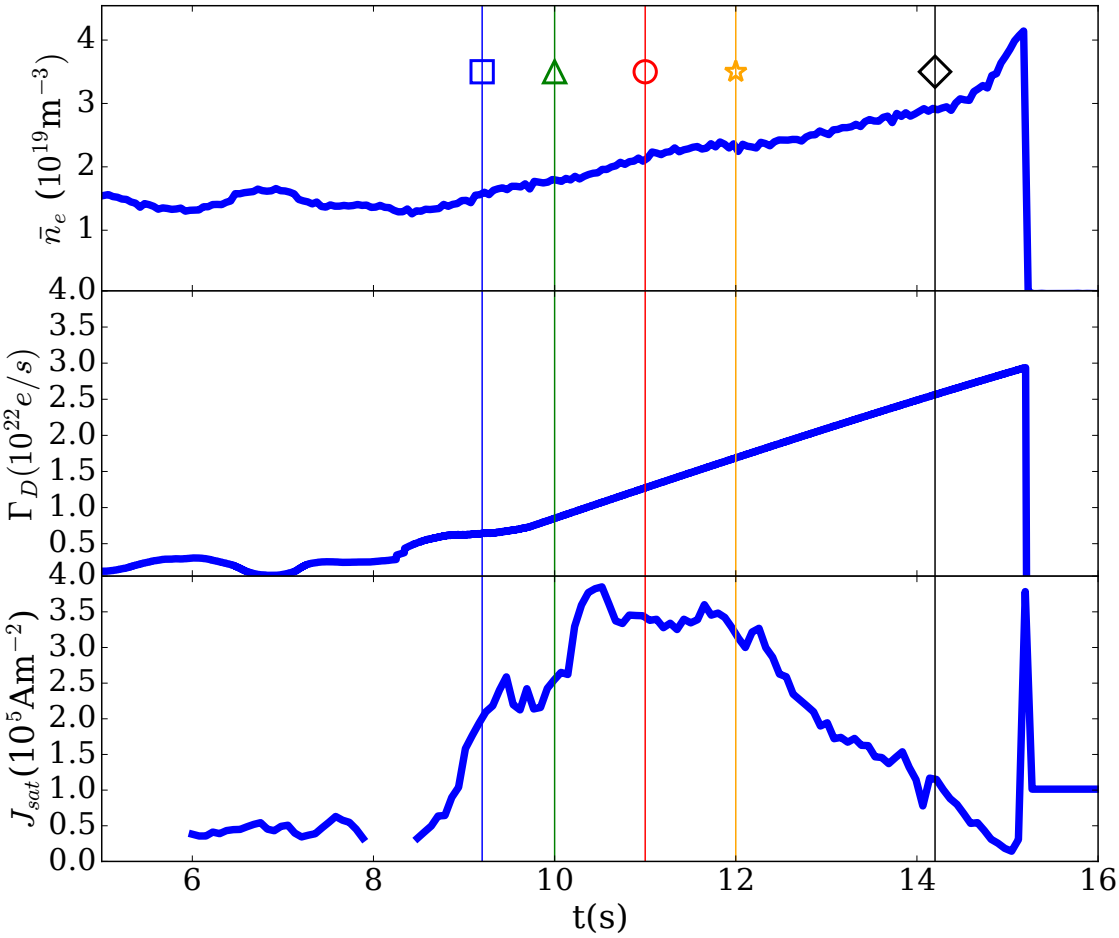

Figure 9:. Time traces of for vertical target L-mode D fuelling ramps at 1.5 MA (JPN 89782). Shown are (a) ñe, $\mathbf{\Gamma}_D$ (b), and strike point J_{sat} ,(c). Detachment is evident in the rollover in J_{sat}. Vertical lines marked with symbols indicate times used for profile shown in figure 10.

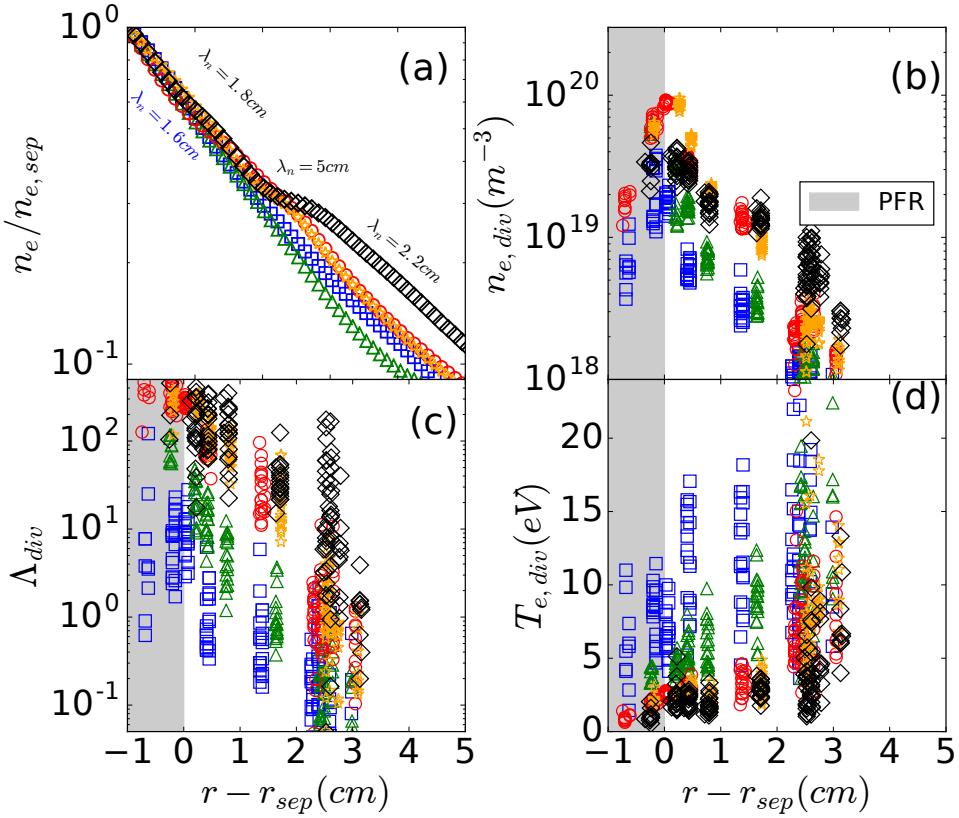

Figure 10: (a) Upstream density profiles, divertor probe data (b & d) and Λ_{div} (c) for a vertical target 1.5MA plasma utilizing a D_2-fuelling ramp to increase $\tilde{n}_e$ (JPN89782). The divertor condition (SL, HR or detached) is different in the near and far SOL. Colours and symbols correspond to the vertical lines and times in figure 9.

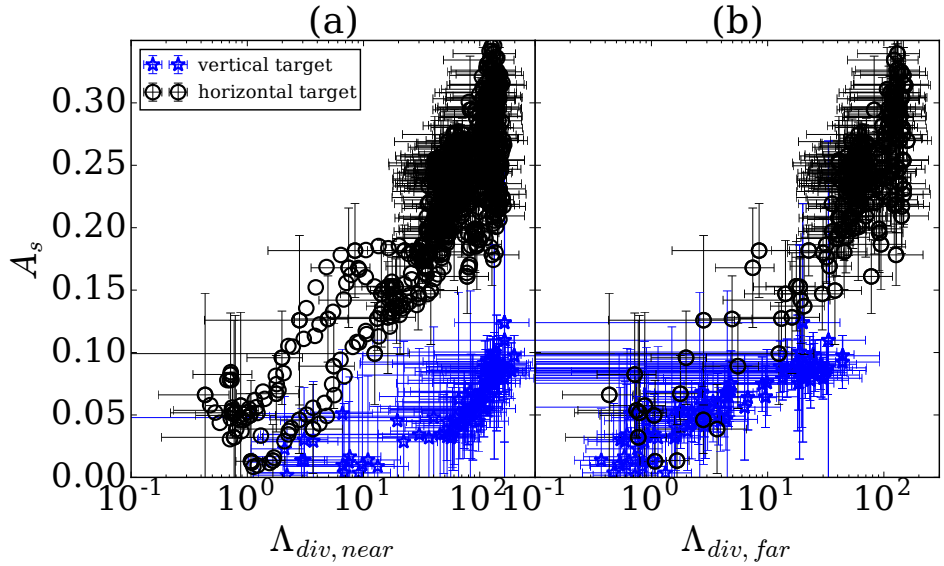

Figure 11: The data is from the same 1.5MA, vertical divertor pulse (JPN89782) as Fig. quadVL2. The correlation between the shoulder amplitude A_s and Λ_{div} in the near (a) and far (b) SOL is given. The data from figure 7 (labeled horizontal target) is also shown for reference.

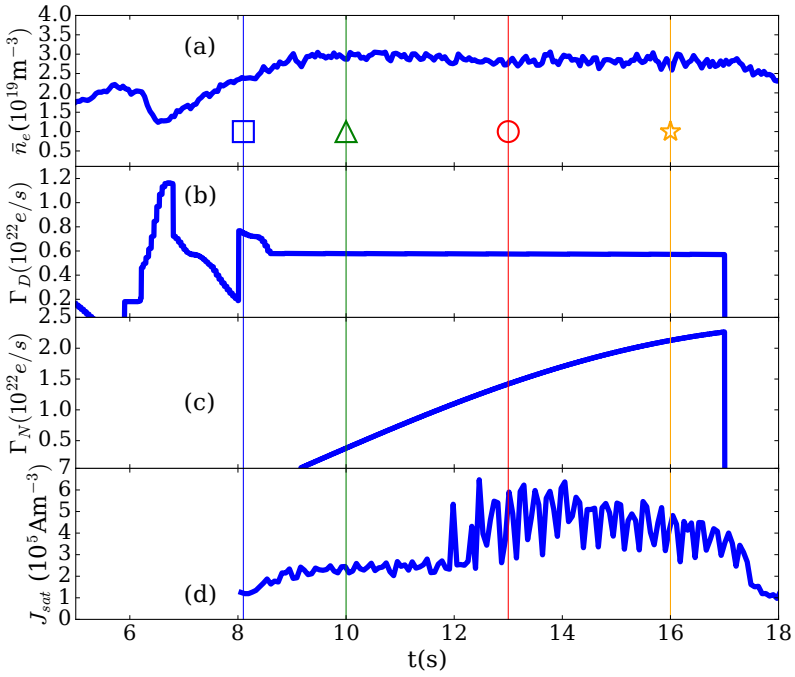

Figure 12: Time traces of N seeding ramps showing (a) ñe, (b) D fuelling rate **Γ**D (c) N seeding rate **Γ**N and strike point density ne,SP. Ip = 2.5MA(JPN90697). Coloured vertical lines marked with symbols

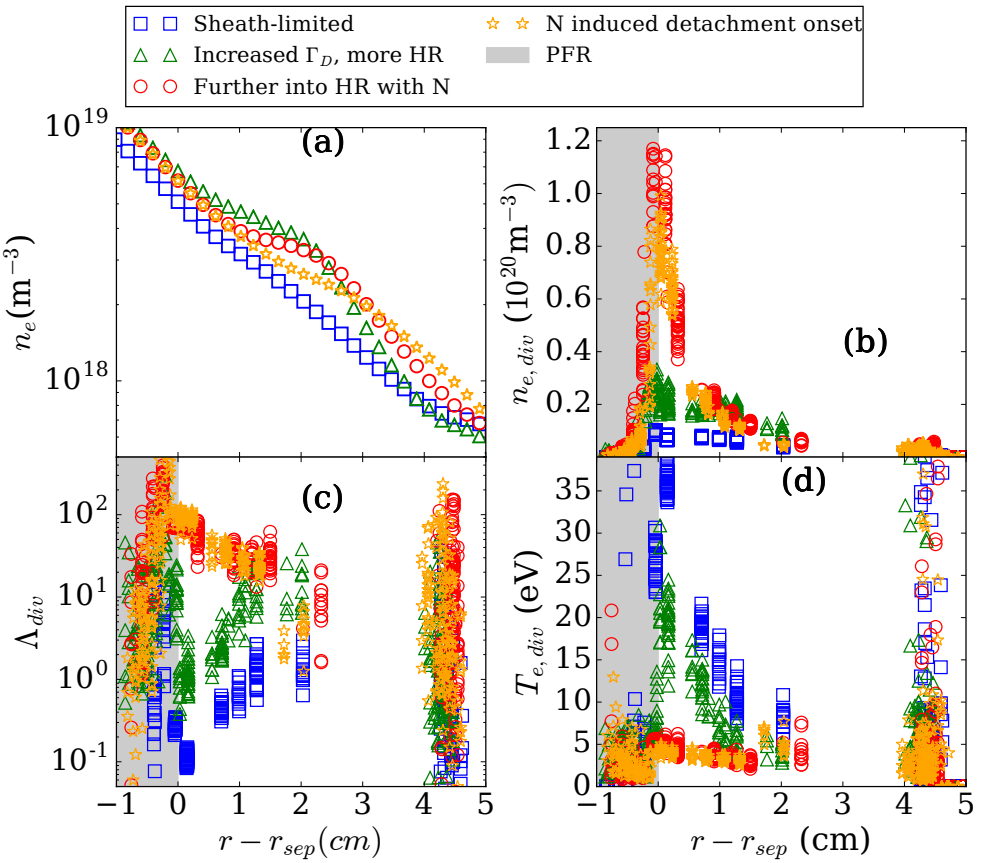

Figure 13: (a) Upstream density profiles, divertor probe data (b-d) and (c) for a horizontal target N seeding ramp, I_p = 2.5MA (JPN90697). Despite strong changes to the divertor conditions due to N seeding, there is only minimal change to the upstream density profile compared. See QuadHL for comparison.

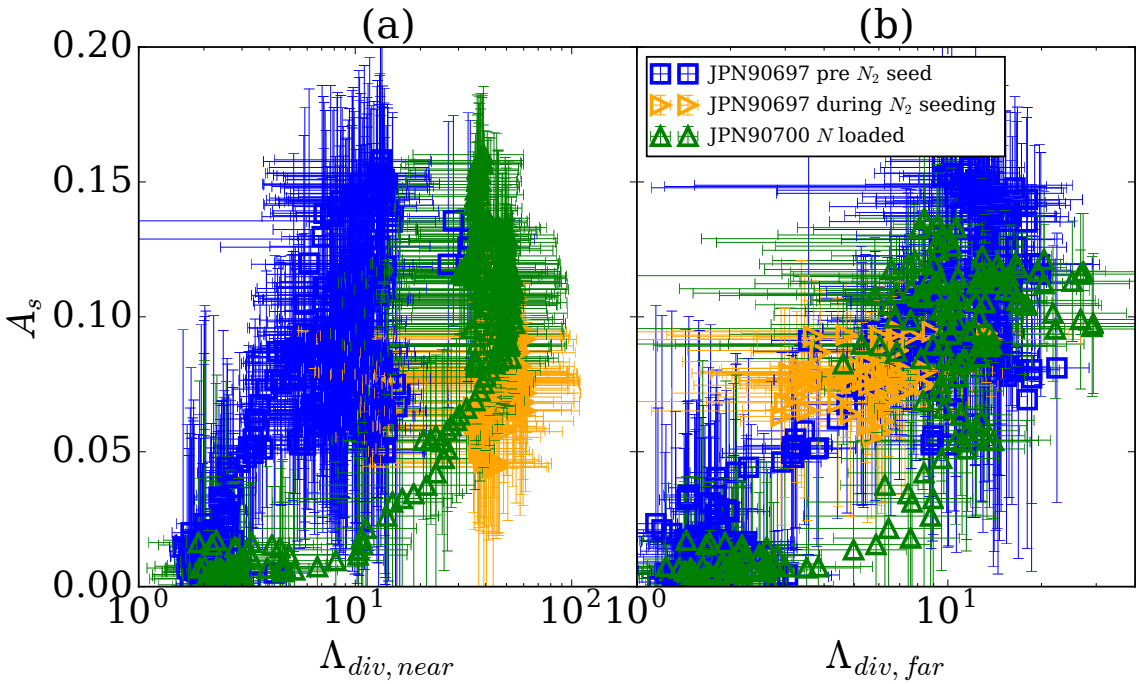

Figure 14: Correlation between the shoulder amplitude A_s with a) $\mathbf{\Lambda}_{div,near}$ and b) $\mathbf{\Lambda}_{div,far}$ for horizontal target before and during unseeded and N_2 seeded periods of pulse JPN90697 as well as for for pulse JPN90700 where the walls are loaded with N from a previous pulse.

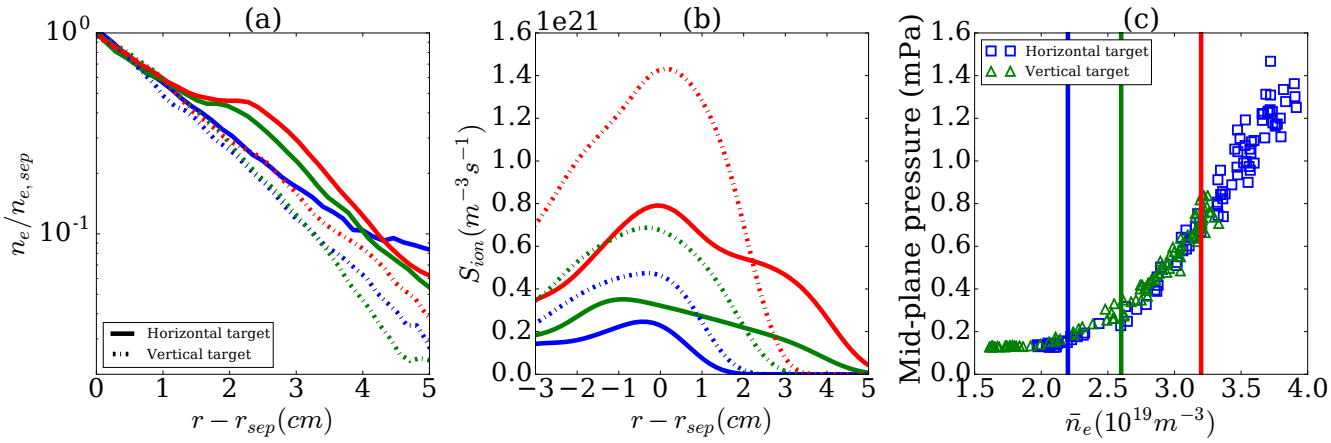

Figure 15: Comparison of normalised density profiles (a) and (b) the localised ionization source (S_{ion}) between horizontal (JPN89346) and vertical target (JPN89783). (c) the mid plane pressure vs line-averaged density. Colours correspond to specific upstream densities as

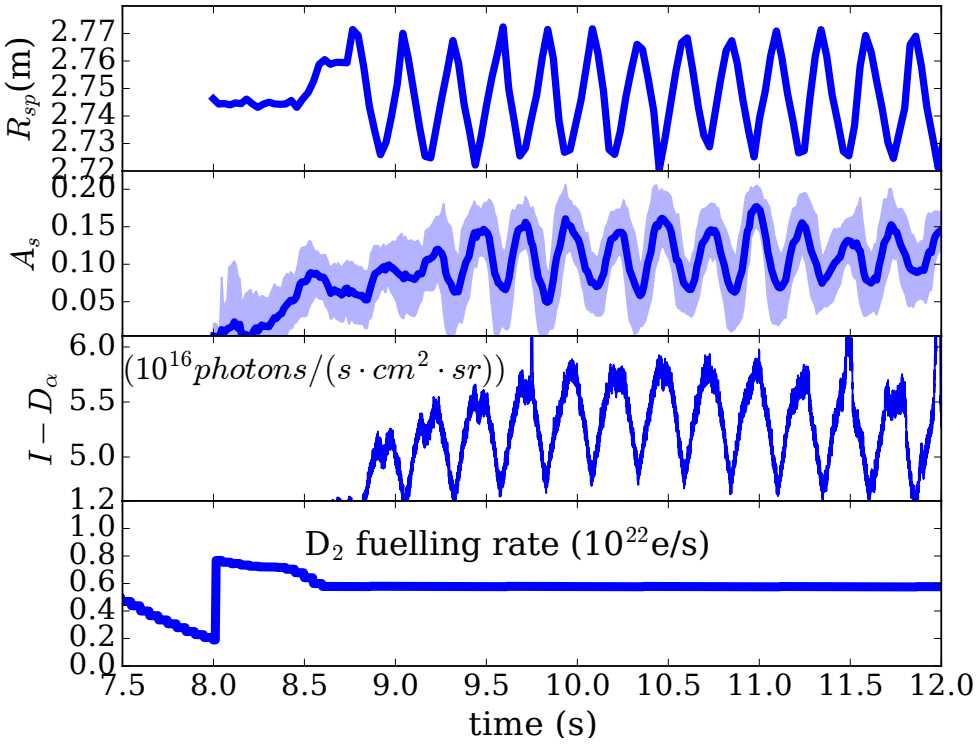

Figure 16: Effect of (a) strike point sweeping on the shoulder amplitude (b) and the outer target D_α emission(c). (d) the D_2 fuelling rate. Data from JPN90697, before N_2 seeding has a significant effect.

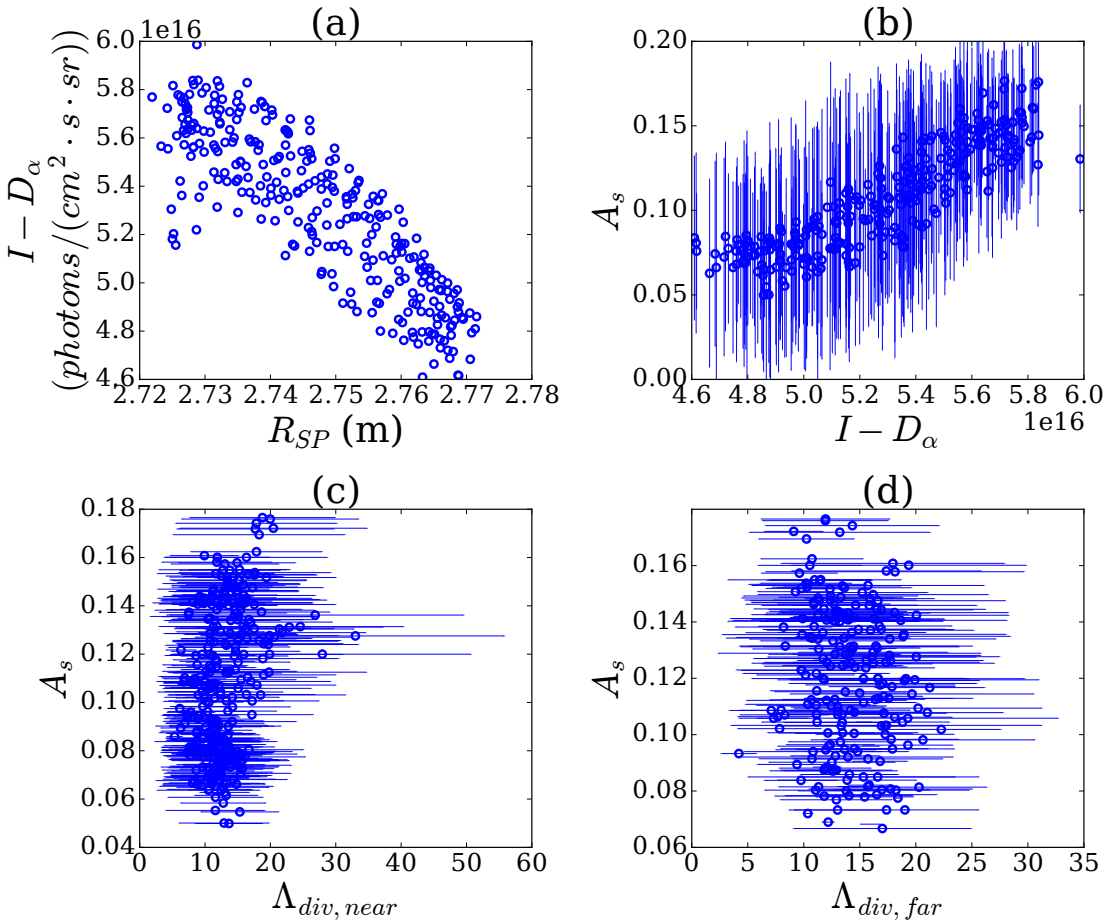

Figure 17: Correlation between the upstream SOL and divertor characteristics, as well as with each other and divertor strike point location, over the period 9-12s for JPN90697. The divertor is in a high recycling condition.

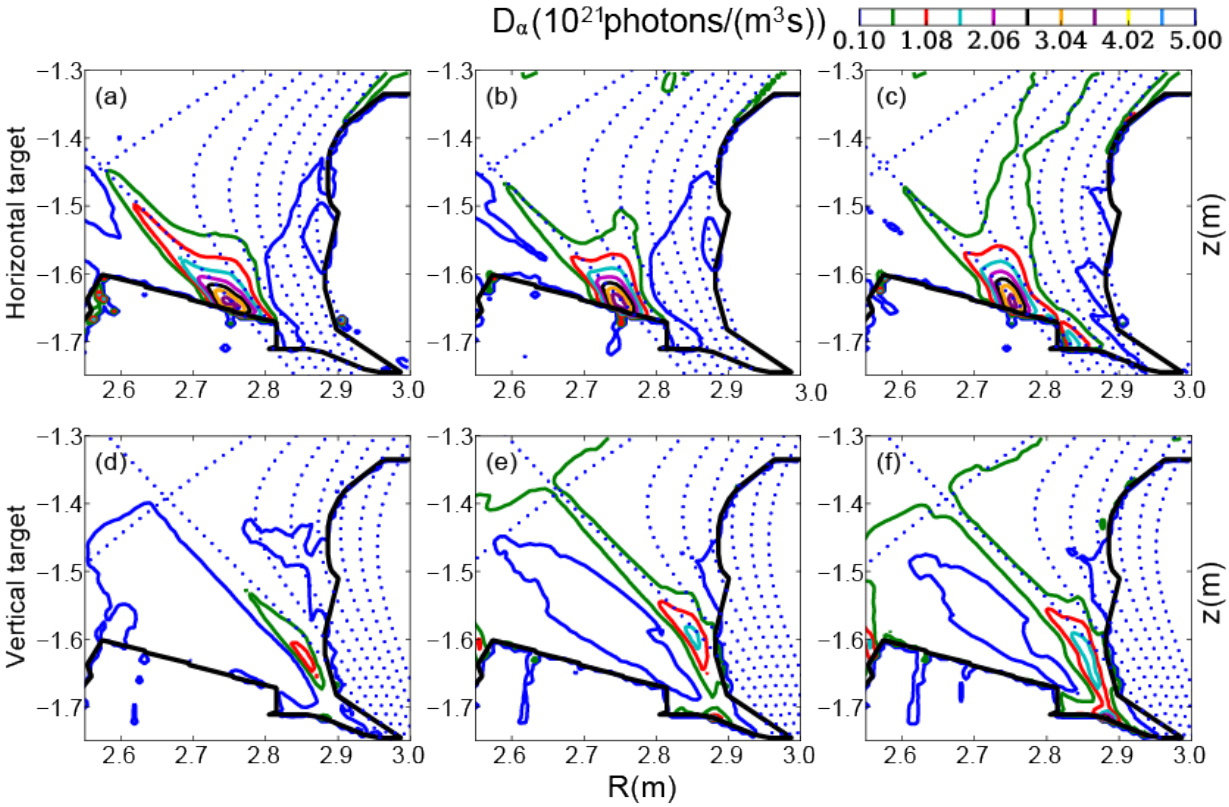

Figure 18: D_α emission contours for horizontal (top row JPN89346) and vertical (bottom row JPN89355) divertor targets. Core densities increase from left to right and are equivalent for each column, the values of which are indicated by vertical lines in figure 15 (c). (a,d) Sheath limited conditions, no shoulder. (b,e) High-recycling conditions with shoulder formation for the horizontal target; (c,f) Divertor conditions are at maximum high-recycling, just before detachment. Shoulder A_s = 0.22 for the horizontal target, no measurable shoulder for the vertical target.

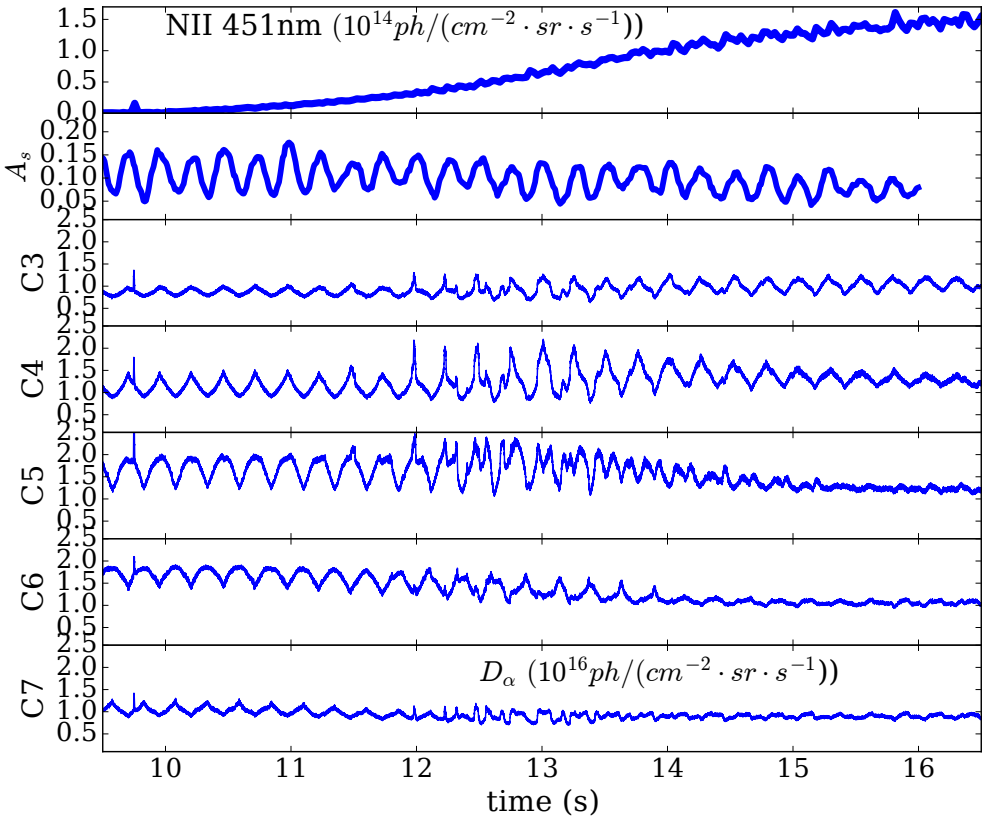

Figure 19: Time traces of (a) NII brightness, (b) Shoulder amplitude A_s and vertical views of the horizontal target (C3-C7; see Figure 2 for details) in D_α brightness are given for JPN90697. The direction of increasing R across the target is C3 to C7. D_2 fuelling is constant over the period shown.

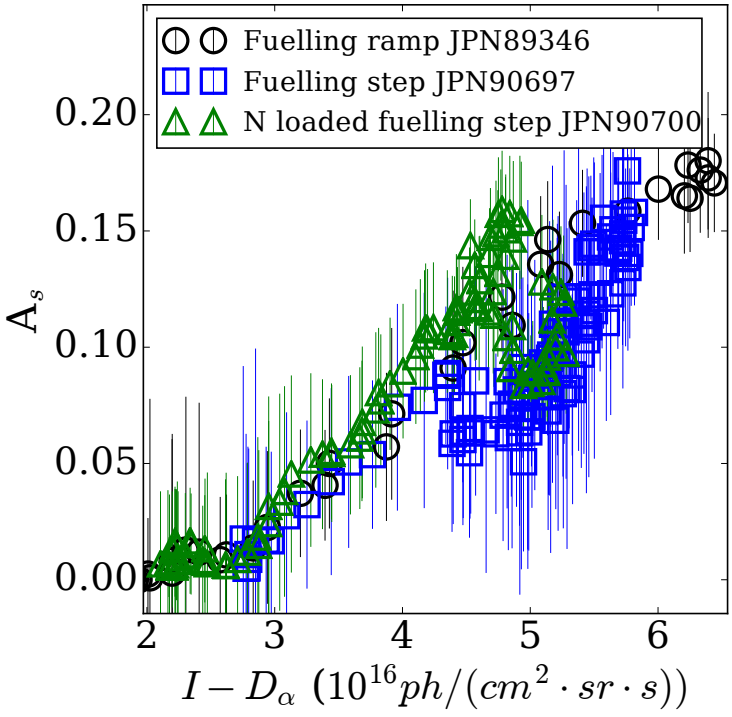

Figure 20: Symbols and colors correspond to figure 14. Correlation between D_α on horizontal target and A_s. The fuelling step is shown in figure 16.

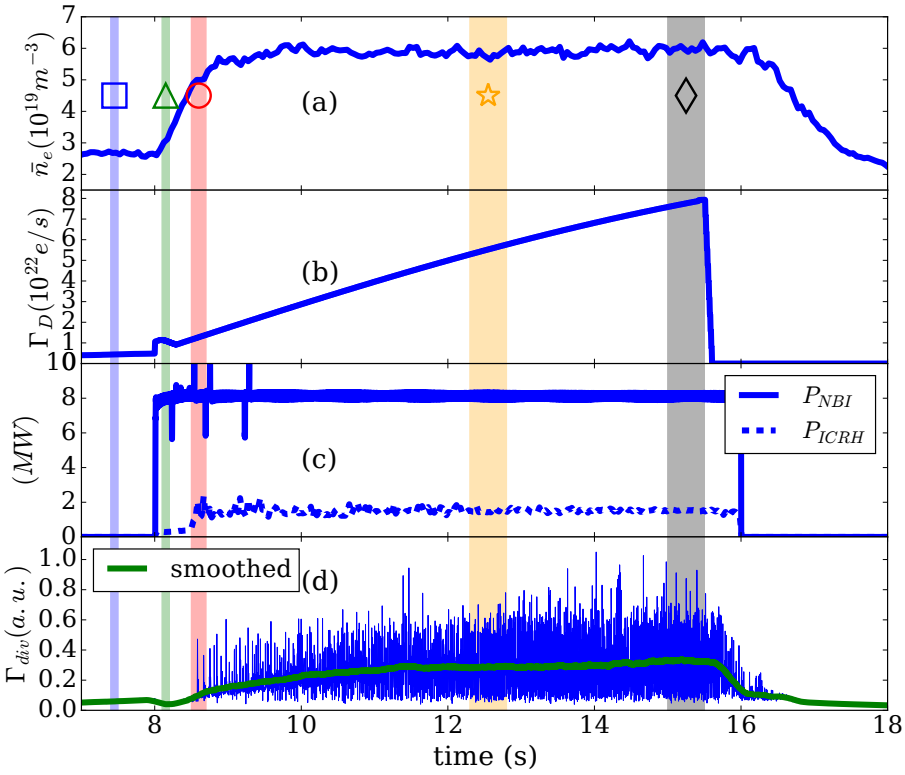

Figure 21: Time traces for a horizontal target D_2 fuelling ramp H-mode (JPN 89786, I_p = 2.2MA). (a) $\tilde{n}_e$ (b) D_2 fuelling rate. Additional heating power from NBI and ICRH (c). Raw and smoothed integrated ion flux to the outer divertor, $\mathbf{\Gamma}_{div}$ (d). Shaded regions marked with symbols indicate times from which inter-ELM profiles are taken. Symbols correspond to figure 23.

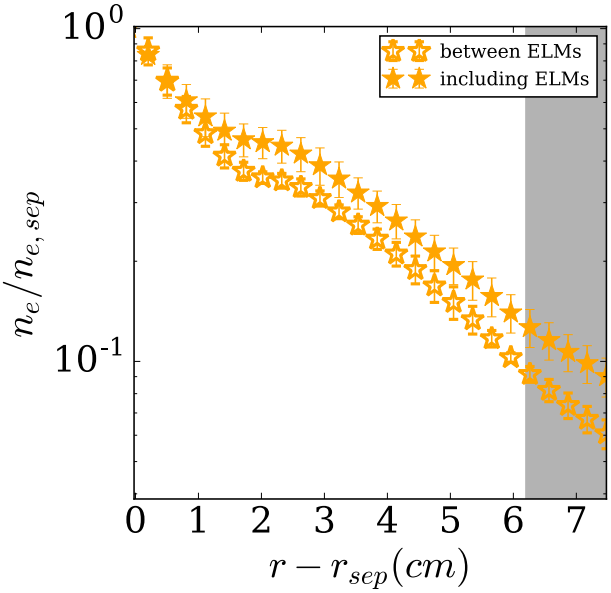

Figure 22: Normalised density profiles averaged over measurements which are either between ELMs or include ELM contributions. The time window over which profiles are taken is shown in figure 21 with corresponding symbols (JPN89786).

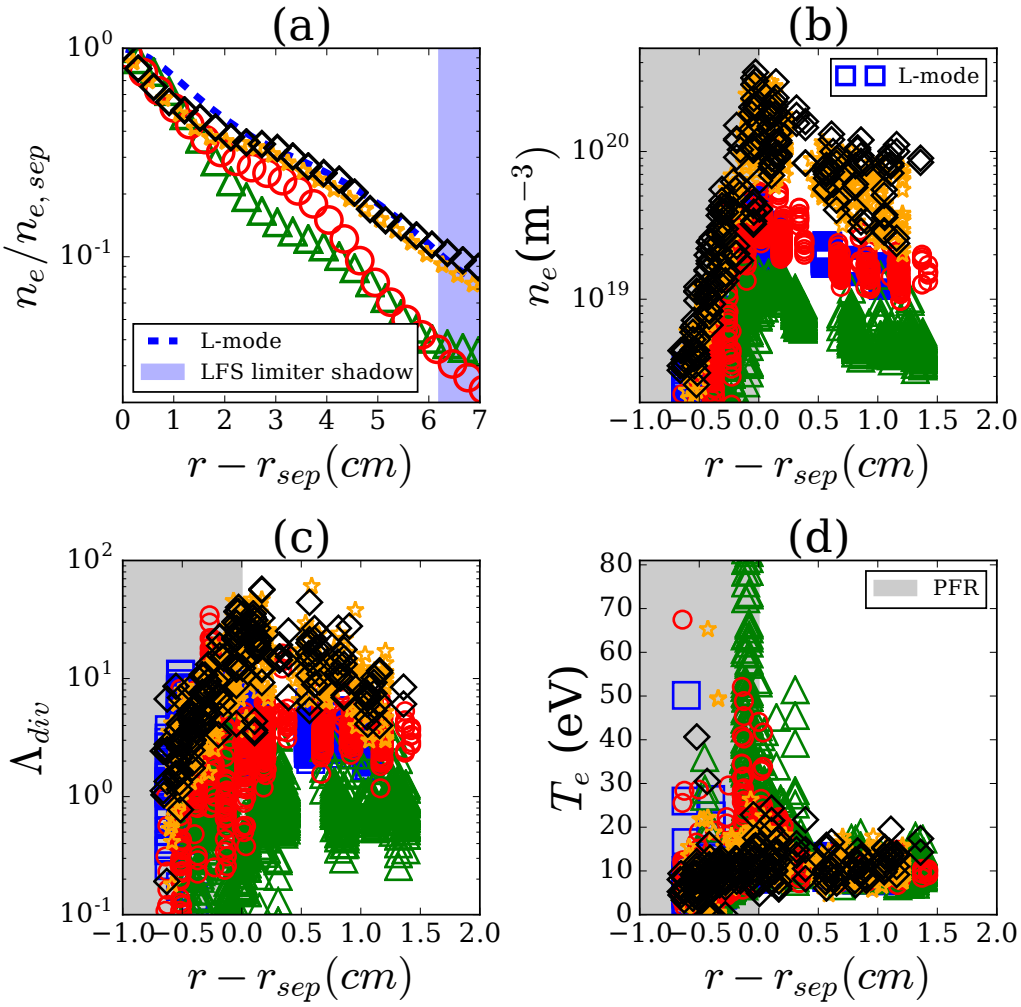

Figure 23: Upstream density profiles (a) and divertor probe data (b,d) along with $\mathbf{\Lambda}_{div}$ (c) for a horizontal target H-mode D fuelling ramp (JPN 89786, I_p = 2.5MA). L-mode data (blue dashed line or squares) is shown for reference. All H-mode profiles are from inter-ELM periods. The probe data has been shifted by +0.25cm such that the peak is at the separatrix. Divertor conditions change from SL to HR, but detachment does not occur. $\mathbf{\Lambda}_{div}$ follows the profile evolution from L-mode to H-mode. Symbols correspond to figure 21.

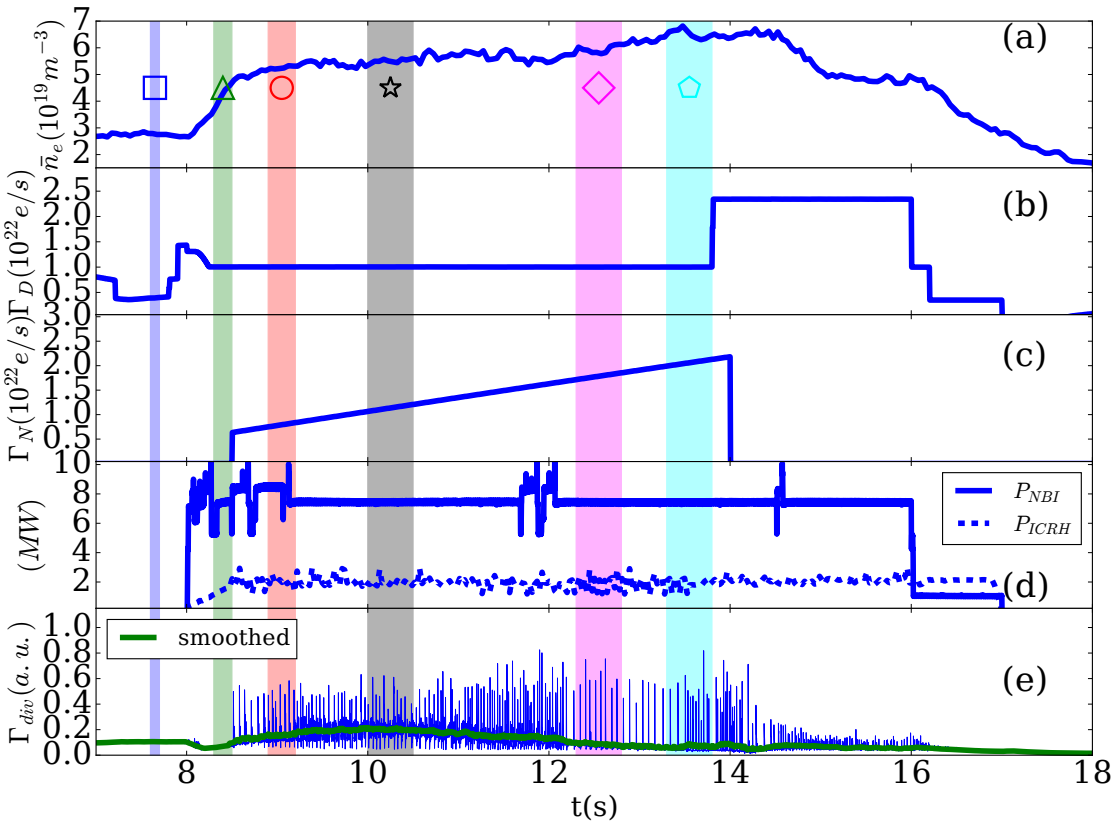

Figure 24: Time traces for a horizontal target H-mode N seeding ramp (JPN 89241,I_p = 2.0MA). Shaded regions marked with symbols indicate times from which inter-ELM profiles are selected. ñe (a) increases at transition to detached conditions (magenta diamonds) and onwards (cyan pentagons). The D_2-fuelling rate, $\mathbf{\Gamma}_D$, is shown along with the N_2-seeding rate, $\mathbf{\Gamma}_N$ (c). Additional heating power from NBI and ICRH (d) are shown along with the total flux to the outer divertor (e), $\mathbf{\Gamma}_{div}$, which drops during detachment.

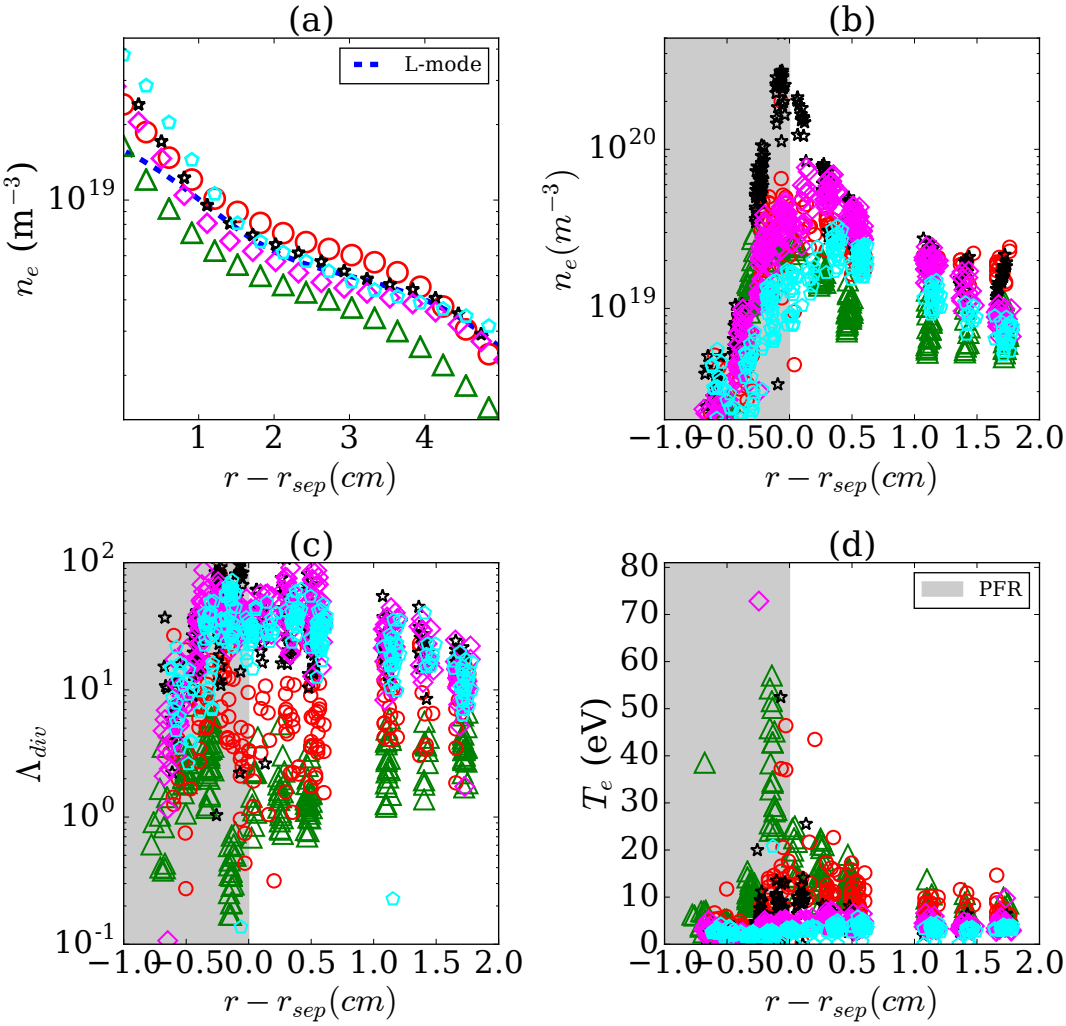

Figure 25: Upstream density profiles (a), divertor probe data (b,d) and $\mathbf{\Lambda}_{div}$(c) for a horizontal target H-mode N seeding ramp (JPN 89241). Symbols correspond to shaded regions in figure 24. Density profiles in (a) are inter-ELM. Strongly detached conditions are achieved due to N seeding, shown by substantial strike point density reductions shown in (b). Density profiles in (a) do not flatten with divertor detachment.